

Session MP-5

Materials/Processes(5)

Adhesion characteristics of underfill material with various package components after plasma and UV/ozone treatments (*Invited*)

Man-Lung SHAM, Mei LAM & Jang-Kyo KIM, Hong Kong University of Science & Technology, Hong Kong

Effect of Heat Treatment on the Interfacial Adhesion Strength between Sn-An-xAg Lead-Free Solders and Cu Substrate

Tao-Chih CHANG, Min-Hsiung HON, National Cheng Kung University, Taiwan

Chin-Hui CHANG, Moo-Chin WANG, National Kaohsiung University of Applied Science, Taiwan

Intermetallic Growth between Sn-Ag-(Cu) Solder and Ni

Seung-Taek YANG, Yun CHUNG, Young-Ho KIM, Hanyang University, Korea

B. H. Hong, K. R. PARK, Amkor Technology Korea, Inc., Korea

H. G. Song, J. W. Moris Jr, U. C. Berkeley, USA

The Effect of Melting Time on Lead-Free Solder Strength

Kari MAATTANEN, Turku Polytechnic, Finland

Jouko HAPPONEN, Aulis TUOMINEN, Pori School of Technology and Economics, Finland

Creep Deformation of Microstructurally Stable Sn-3.5Ag-xBi Solders

S. W. SHIN, J. YU, Korea Advanced Institute of Science and Technology, Korea

Adhesion characteristics of underfill material with various package components after plasma and UV/ozone treatments

Man-Lung SHAM, Mei LAM & Jang-Kyo KIM
Department of Mechanical Engineering
Hong Kong University of Science & Technology
Clear Water Bay, Hong Kong
E-mail: meivan@ust.hk

Abstract

The role of underfill in enhancing the reliability of flip chip packages is of paramount importance, particularly for the low-cost packages made of organic printed circuit boards. Amongst many reliability issues in flip chip packages, delamination between the underfill and other package components is detrimental to the mechanical and functional performance of the package because delamination often leads to premature failure of the whole device. In the present study, the interfacial bond strengths of both conventional and no-flow underfill resins with die passivation, solder and polyimide soldermask are measured based on the button shear test; and the surface characteristics of these substrates are analysed using several analytical tools, including the atomic force microscopy, X-ray photoelectron spectroscopy and contact angle measurement. Plasma and UV/ozone treatments are applied before encapsulation to improve the underfill-package components interface bond. It is found that the interfacial bond strength of underfill with solder was the weakest, while it was highest with silicon nitride passivation layer amongst the above substrates studied. Both plasma and UV/ozone treatments improved the interfacial bond strength with polyimide soldermask along with a decrease in contact angle of the surface. Among the various thermodynamic parameters the spreading coefficient was shown to have close correlation with the underfill-solder interfacial bond strength. The significance of this finding is discussed.

Introduction

Although the use of underfill encapsulation improves significantly the reliability of solder joint interconnection in flip chip packages, delamination at various interfaces remains a major concern. This is because delamination of underfill degrades the solder joint reliability by magnifying the solder deformation under cyclic loading. Delamination also results in accumulation of moisture at the failed interfaces leading to additional failure modes [1]. Many approaches have been developed to improve the interface adhesion, which include addition of silica fillers in underfill to reduce the thermal mismatches between the package components, incorporation of silane coupling agent in underfill resin, and modification of the surface properties of the package components based on plasma or UV/ozone treatment.

Apart from the modification of material intrinsic properties to enhance the interfacial bonding, there are also a number of methods to evaluate the bonding quality. The formation of a strong interface bond begins with the establishment of intimate interfacial molecular contacts through wetting the substrate by the liquid phase, along with minimum interfacial defects. Gent & Schultz [2] suggested that the interface bond strength is proportional to the work of adhesion and the plastic work of the viscoelastic adhesive during fracture. The work of adhesion, W_a , is the energy required to separate reversibly the interface between the two phases:

$$W_a = \gamma_1 + \gamma_2 - \gamma_{12} \quad (1)$$

where γ_1 , γ_2 and γ_{12} are the surface tensions of solid phase 1, liquid phase 2 and the interfacial tension between these phases, respectively. In fact, the extent of wetting of one phase by another is best illustrated by the contact angle phenomena. The contact angle of a sessile drop of a liquid on a solid surface, θ_y , corresponds to the lowest energy state of the system, which is described by the well-known Young's Equation.

$$\gamma_2 \cos \theta_y = \gamma_1 - \gamma_{12} \quad (2)$$

Combining Equation 1 with 2 yields

$$W_a = \gamma_2 (1 + \cos \theta_y) \quad (3)$$

Although there is correlation between the work of adhesion and practical interface bond strength [3], a number of discrepancies were reported [3, 4]. Instead, Mittal [3] suggested that such a relationship would be invalid when the adhesive completely wetted the substrate before the solidification of the adhesive. Apart from the work of adhesion, Wu [5-6] also proposed the spreading coefficient, (S_{21}), which is defined as the decrease in free energy per unit area covered by the liquid phase 2 on the substrate phase 1:

$$S_{21} = \gamma_1 - \gamma_2 - \gamma_{12} = W_a - 2\gamma_2 \quad (4)$$

A positive S_{21} value is required for spontaneous spreading of the liquid phase onto the substrate surface. In other words, the work of adhesion, W_a , should be greater than the cohesive energy of liquid, $2\gamma_2$, for complete wetting of substrate by the liquid phase [4]. The spreading coefficient was shown to correlate well with the interface bond strength [3, 5]. Mittal [3] further proposed the interfacial tension was probably one of

the most significant surface energetic parameters in determining the interface bond strength: the lower the interfacial tension the higher the spreading coefficient, and the higher the interface bond strength. Apart from the wettability theory in explaining the adhesion, there are many other sources of adhesion, namely, mechanical interlocking, interdiffusion and interpenetrating network concepts, and chemical bonding theory [7].

It is well accepted that there is no single adhesion mechanism responsible for the total interfacial bond strength, and the relative importance depends on the individual substrate-adhesive systems [7]. Hence, understanding the whole flip chip package interface is very difficult because of many different interfaces involved. For example, the underfill-passivation system is polymer/ceramic or polymer/polymer interface in nature, depending on the passivation employed, e.g. silicon oxide, silicon nitride and benzocyclobutene (BCB). It is well documented that the interface between the underfill and passivation layer is prone to delaminate under thermal cycling [8-9], humidity test [10], or destructive test [11-13]. Besides modifying the constituents of underfill material, additional surface treatments of passivation layer, such as incorporating a silanol or amine group into the layer [13-14] or increasing the surface roughness [14], were further proposed to improve the interface bond strength. On the other hand, the underfill-soldermask interface constitutes polymer/polymer adhesion, where diffusion-assisted chemical reactions may take place accompanied with some mechanical interlocking. The adhesion of underfill with soldermask would be severely degraded when exposed to hygrothermal environment [13,15], as well as when subjected to surface contamination due to flux residue [16] or residues remained after wet cleaning [17]. Plasma cleaning [18-21] and UV/ozone cleaning [22-23] were employed to restore the degraded interfacial bond.

Relatively little attention has hitherto been given to the interfacial bond strength between underfill and solder joints. It is noted [24] that underfill delamination was typically initiated from the region near solder joint corners during thermal cycling, which is likely to be associated with the local CTE mismatch between the two components. Numerical analyses [25-26] confirmed the detrimental effect of total debonding between the underfill and solder bump on the device reliability. On the other hand, surface oxidation over the solder joints with varying degrees of tin oxide [27] and aging under humid conditions [28] also deteriorated the interfacial bond strength significantly.

As a continuation of our previous study on characterizing the underfill adhesion [26], the interfacial bond strengths of conventional and flux-containing no-flow underfills with silicon passivations, soldermask, plasma cleaned soldermask, and eutectic solder material were measured in the button shear test. In order to determine the factors governing the interface bond strength, the surface roughness, surface chemical compositions and thermodynamic surface energetics were measured using the atomic force microscopy

(AFM), X-ray photoelectron spectroscopy (XPS) and contact angle method. Attempts were made to establish the correlation between various thermodynamic parameters and the interfacial bond strength.

Experimental Procedure

In this study, two conventional and two no-flow underfill resins (supplied by Dexter, Loctite and National Starch) were processed according to the recommended curing conditions given in Table 1. The composition and specifications of the substrate surfaces are summarised in Table 2. The plasma treatment on soldermasks was performed using an Edwards Thermal Evaporation System Auto306 for 10 min. in argon gas, while UVO/cleaner (Model 144AX-22) was employed to expose the soldermask surface to UV/ozone for 5 min. The specimen dimensions and testing conditions for the button shear test are shown in Figure 1. A shear load was applied at a speed of 50 μ m/s using a blade 250 μ m above the substrate surface on a Dage 4000 Multi-purpose Bond Tester.

Table 1. Curing conditions for the underfills

| Underfill | Conventional | | No-flow | |
|------------------------------------|--------------|----|---------|----|
| | A | B | C | D |
| Curing Temperature ($^{\circ}$ C) | 16 | 15 | 16 | 1 |
| Curing Time (min) | 0 | 0 | 5 | 60 |
| | | | | 6 |
| | 7 | 30 | 10 | 0 |

Table 2. Substrates under investigation for adhesion test.

| Substrates | Specifications |
|-----------------------------|---|
| Soldermask | Taiyo 4000 polyimide soldermask |
| Solder plate | 63/37 Sn/Pb |
| Silicon Dioxide Passivation | Passivation layer of 0.75 μ m on the bare die of 525 μ m in thickness |
| Silicon Nitride Passivation | Passivation layer of 0.75 μ m over the bare die of 525 μ m in thickness |

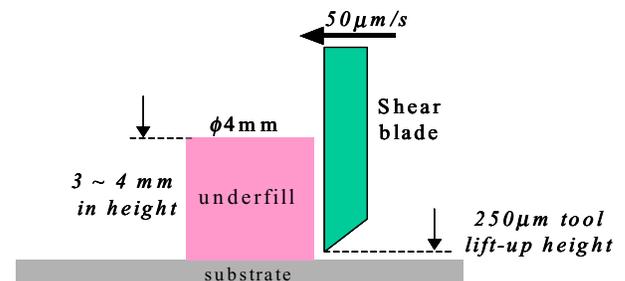


Figure 1. Schematic drawing of the button shear test.

The surface energies of the substrate and cured underfill surfaces were determined by measuring the contact angles, θ_y , of de-ionized (DI) water and methylene iodide using a Krüss G10 contact angle measuring system. The polar and non-polar

(or dispersive) components, γ_1^p and γ_1^d , respectively, of surface energy were evaluated based on the harmonic-mean approach [5].

$$\gamma_{21}(1 + \cos\theta_y) = \frac{4\gamma_1^d\gamma_2^d}{\gamma_1^d + \gamma_2^d} + \frac{4\gamma_1^p\gamma_2^p}{\gamma_1^p + \gamma_2^p} \quad (5)$$

The polar and dispersive components of surface energy of the measuring liquids, γ_2^p and γ_2^d , are 22.1 and 50.7 for DI water, and 44.1 and 6.7 for methylene iodide, respectively. Therefore, the interfacial tension, γ_{12} , was determined based on:

$$\gamma_{12} = \gamma_1 + \gamma_2 - \frac{4\gamma_1^d\gamma_2^d}{\gamma_1^d + \gamma_2^d} - \frac{4\gamma_1^p\gamma_2^p}{\gamma_1^p + \gamma_2^p} \quad (6)$$

Results and discussions

Button shear test results

Figure 2 summarises the interfacial bond strengths and the corresponding failure mechanisms of the four underfills with various package components. These failure mechanisms are schematically presented in Figure 3. The interface bond strength between the underfill and solder material was the weakest among the substrates studied, regardless of type of underfill resin. The failure took place predominantly along the underfill-solder interface (Figure 3(a)). With a such weak interface bond strength, the underfill/solder interface is most likely the location where debonding would initiate preferentially during/after cyclic loading, as confirmed by the numerical analysis [26].

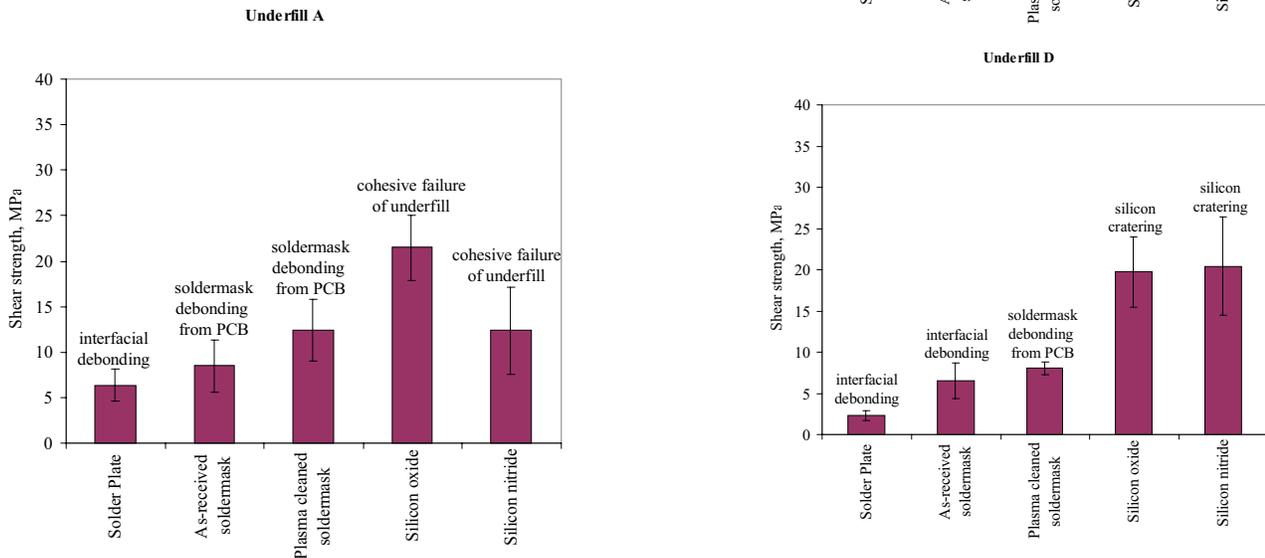


Figure 2. Interfacial bond strengths of underfill with various substrates.

The failure mechanisms and the corresponding interfacial bond strengths of the underfill-soldermask system were dependent significantly on the type of underfill used. The conventional underfill interface failed predominantly by delamination along the soldermask-printed circuit board interface, rather than the underfill-soldermask interface (see Figure 3(b)). This indicates a much stronger bond for the latter interface than for the former. In contrast, the no-flow underfill resins tended to debond along the interface with soldermask, with generally lower interfacial bond strengths than for the conventional underfill resins.

Totally different failure mechanisms were observed with the die passivation layers. The conventional underfill failed cohesively with cracks propagating right through the underfill itself (Figure 3(c)). In contrast, cracks tended to propagate through the die, forming a crater on the fracture surface of the samples with no-flow underfill (Figure 3(d)). The interfacial bond strengths of no-flow underfill with passivation were consistently higher than that of the conventional underfill, and these observations held for both the silicon oxide and silicon nitride passivation layers. Therefore, the no-flow underfill gave the highest interfacial bond strength with passivation layers amongst the substrates studied. Strong chemical bonds between the organosilane coupling agent added in the epoxy-based underfill and the hydroxyl group on the passivation surface were mainly responsible for the underfill-passivation interfacial bond [29-30], as schematically drawn in Figure 4. In particular, the silicon oxide passivation may form a C-O-Si and/or C-Si covalent bond with the resin [31] which is absent in the other systems.

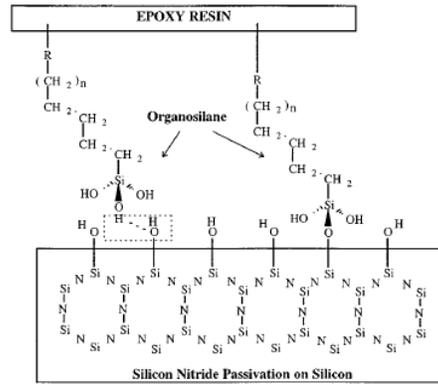


Figure 4. Bonding mechanisms of organosilane in the epoxy resin with silicon nitride passivation [30].

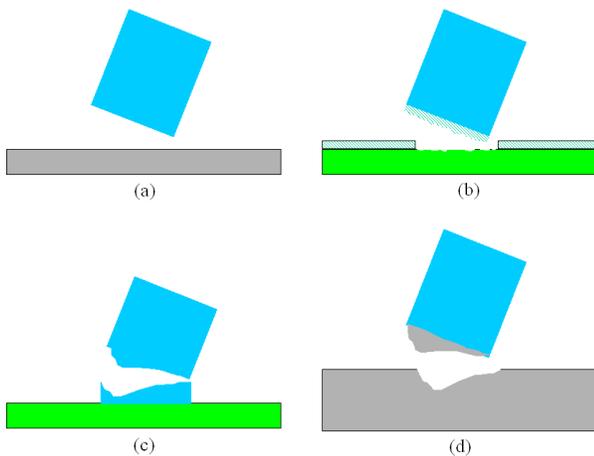
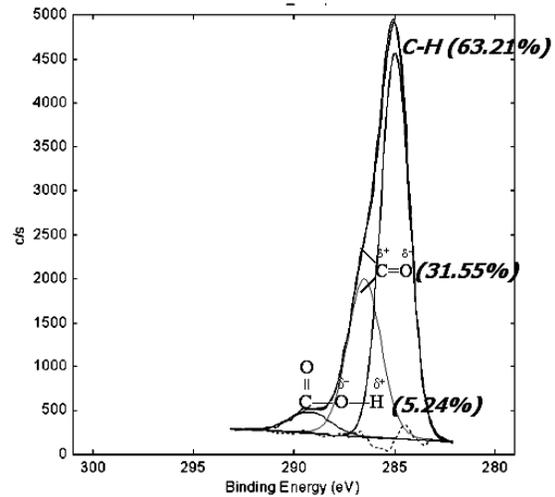
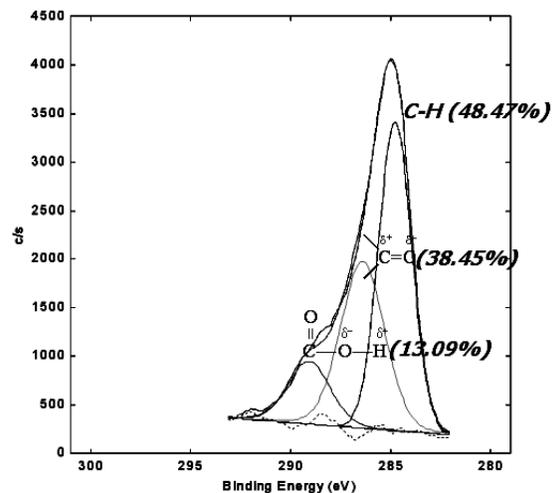


Figure 3. Schematics of different failure modes in button shear test: (a) interfacial failure; (b) soldermask debonding; (c) cohesive failure within underfill; and (d) silicon cratering



(a) As-received



(b) Ar Plasma treated

Figure 5. XPS analyses on soldermask: (a) before; and (b) after argon plasma treatment.

Surface analyses on soldermask

Soldermask plays a key role in protecting the copper traces from mechanical scratches, corrosion as well as oxidation arising from the solder bumping/reflow processes. For these reasons, soldermask is indispensable in low-cost flip chip packages and thus the adhesion performance of soldermask with encapsulant/underfill is important. Plasma treatment of soldermask has been widely used to enhance the interfacial bond strength. Besides removing the surface contaminants arising from wet cleaning, plasma treatment improved the surface wettability by increasing the polar component of surface energy and also was able to roughen the surface during the physical bombardment of heavy ions, enhancing the mechanical interlocking [32].

The atomic force microscopy (AFM) was performed to study the substrate surface morphology and the roughness. The result indicates that the average surface roughness of soldermask increased from 56nm to 70nm after plasma treatment, which was significantly higher than the roughness of die passivation (around 2nm). This observation suggests that the surface roughness was not the principal determining factor for interfacial bond strength of passivation layers with underfill.

The atomic compositions of substrate surface were obtained from the X-ray photoelectron spectroscopy (XPS). Figure 5 shows the deconvoluted XPS spectra for the soldermask surfaces before and after the plasma treatment, and Table 3 summarises the corresponding elemental compositions and the interfacial bond strengths. The decrease in carbon and increase in oxygen contents

suggest that the Ar plasma treatment not only removed the contaminants on the soldermask surface, but it also induced breakage of C-C and C-H bonds, in turn allowing double bonds to form (i.e. crosslinking) and trapping of radicals [33]. Hence, more oxygen from air was incorporated with the long-lived radicals on the soldermask surface after the plasma treatment, as confirmed by the increase in oxygenated functional groups.

Correlation between interfacial bond strength and thermodynamic parameters

The surface free energies of substrate were evaluated by measuring the contact angles in a sessile-drop test. Using Equation 5, the polar and non-polar components of surfaces were obtained and summarized in Table 4. Polarity is defined as the ratio of the polar component, γ^p , to the total surface energy, γ^s . A number of points arise for discussion. The polar component of the soldermask surface energy increased significantly after plasma treatment, which was thought to be attributed to the removal of surface organic contaminant, as well as the incorporation of oxygenated polar groups [34]. The contact angle measurement results (Table 4) agree well with the XPS analyses (Table 3) before and after plasma treatment. The increased polar groups enhanced the wettability and allowed possible sites for covalent bonds to form during the underfill curing, thence stronger interfacial bonds as seen in the present work and others [32]. When compared to the plasma treatment, the UV/ozone treatment was slightly less effective in improving the total and polar component of surface energy. A rather reversed observation can be made for the UV/ozone treated passivation layers. Both the polar and

Table 3. Atomic compositions and interface bond strengths of solder with and without plasma treatment

| | XPS analysis | | | | | Polarity from contact angle measurement | Button shear test | | | | | |
|-------------------------|------------------------|-------|-------|------|------|---|-------------------------------|--------|-------|-------|-------|------|
| | Atomic composition (%) | | | | | | Interface bond strength (MPa) | | | | | |
| | C1s | O1s | N1s | Si2p | O/C | | A | B | C | D | | |
| Before Plasma Treatment | 68.30 | | 22.53 | | 0.92 | 8.26 | 0.33 | 15.68% | 8.48 | 14.56 | 4.33 | 6.46 |
| | C-H | C=O | COOH | | | | | | | | | |
| | 68.21 | 31.55 | 5.24 | | | | | | | | | |
| | C1s | O1s | N1s | Si2p | O/C | | | | | | | |
| After Plasma Treatment | 48.17 | | 40.70 | | 2.49 | 8.63 | 0.84 | 55.30% | 12.39 | 12.41 | 10.05 | 8.02 |
| | C-H | C=O | COOH | | | | | | | | | |
| | 48.47 | 38.45 | 13.09 | | | | | | | | | |

Table 4 Polarity of various package component surfaces and cured underfill.

| Unit: mJ/m ² | | γ^p | γ^d | γ^s | Polarity (γ^p/γ^s) |
|-----------------------------|--------------------------|------------|------------|------------|----------------------------------|
| Solder plate | as-received | 14.20 | 29.89 | 44.09 | 0.32 |
| | ozone-cleaned | 9.15 | 32.53 | 41.68 | 0.22 |
| Soldermask | as-received | 5.53 | 30.37 | 35.90 | 0.15 |
| | plasma cleaned | 39.16 | 31.66 | 70.81 | 0.55 |
| | ozone cleaned soldermask | 16.87 | 24.57 | 41.44 | 0.41 |
| Silicon oxide passivation | as-received | 41.66 | 25.19 | 66.85 | 0.62 |
| | ozone cleaned | 25.46 | 23.80 | 49.26 | 0.52 |
| Silicon nitride passivation | as-received | 34.76 | 26.28 | 61.04 | 0.57 |
| | ozone cleaned | 33.68 | 24.82 | 58.50 | 0.58 |
| Underfill A | | 11.28 | 29.74 | 41.02 | 0.27 |
| Underfill B | | 10.24 | 33.74 | 43.98 | 0.23 |
| Underfill C | | 6.89 | 40.86 | 47.75 | 0.14 |
| Underfill D | | 14.04 | 35.27 | 49.31 | 0.28 |

dispersive components of surface energy decreased after the treatment, an indication of more contaminated substrate surface due probably to overexposure. This resulted in a reduction of work of adhesion even though the interfacial energy also decreased after the UV/ozone treatment, as shown in Table 5. Several thermodynamic parameters have been successfully used to correlate with the practical interfacial bond strength, for instance, work of adhesion [3,35], analogous surface energies [3,36] and polarities between adhesive and substrate [3, 5], interfacial tension [3,5], spreading coefficient [3,5], etc. Table 5 summarises the calculated values of these parameters for various combinations of underfill and substrate surface. The interfacial bond strengths are also included where available. Judging from the various failure mechanisms for different substrate surfaces (Figure 3), only the underfill-solder interface showed strictly adhesive failure, which satisfies the requirement for correlating the thermodynamic parameters with the practical interfacial bond strength. It is interesting to note a linear variation of the interfacial bond strength with the spreading coefficient, as shown in Figure 6. The higher the spreading coefficient the stronger the interface bond was [5].

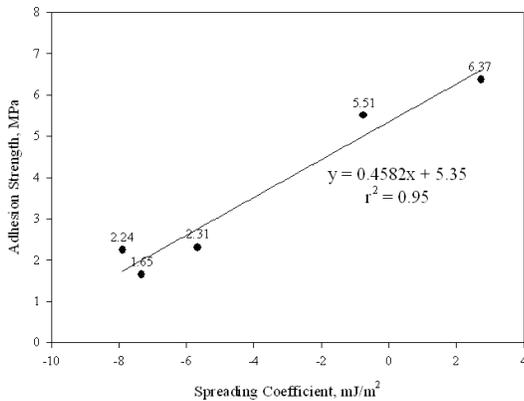


Figure 6. The correlation between spreading coefficient and interfacial bond strength of various underfill resins on solder material.

Concluding Remarks

The button shear test and contact angle measurements were performed together with the AFM and XPS analyses to evaluate the interfacial bond strength of underfill with various flip chip substrate surfaces. The following remarks can be drawn from this study.

1. All underfill resins exhibited the weakest interfacial bond strength with solder material, indicating preferential delamination along this interface when the package is subjected to cyclic loading.
2. A majority of underfill resins showed better interfacial bond strengths with passivation layers than with soldermask.
3. The interface bond strength of underfill with soldermask was improved after argon plasma and UV/ozone treatments, due to the removal of surface contaminants arising from wet cleaning as well as the incorporation of polar groups promoting chemical reactions with the underfill.
4. The spreading coefficient showed a linear correlation with the practical interfacial bond strength of underfill with solder material.

Acknowledgements

The work described in this paper was partially supported by grants from the Research Grants Council of the Hong Kong Special Administrative Region, China (Project No. HKUST 6014/98E and DAG 00/01. EG18). Technical supports from the Materials Characterization and Preparation Facilities (MCPF) and EPack Laboratory of HKUST are appreciated.

References

1. Gektin, V., Bar-Cohen, A. & Witzman, S., "Coffin-Manson based fatigue analyses of underfilled DCAs", *IEEE Trans on CPMT-Part A*, vol. 21, No. 4, Dec. (1998), pp.577-584.
2. Gent, A.N. & Schultz, J., "Effect of wetting liquids on the strength of adhesion of viscoelastic materials", *J. Adhesion*, vol. 3 (1972), pp.281-294.
3. Mittal, K.L., "Surface chemical criteria for maximum adhesion and their verification against the experimentally measured adhesive strength values", *Adhesion Science &*

Table 5. Thermodynamic parameters on adhesion from contact angle analysis.

| | Underfill A | | | | Underfill B | | | | Underfill C | | | | Underfill D | | | |
|--|---------------|-------|--------|----------|---------------|-------|--------|----------|---------------|-------|--------|----------|---------------|--------|--------|----------|
| | γ_{12} | W_a | ρ | σ | γ_{12} | W_a | ρ | σ | γ_{12} | W_a | ρ | σ | γ_{12} | W_a | ρ | σ |
| Solder | | | | | | | | | | | | | | | | |
| As-received | 0.34 | 84.77 | 0.84 | 6.37 | 0.87 | 87.2 | 0.72 | 5.51 | 4.23 | 87.61 | 0.44 | 2.24 | 0.45 | 92.95 | 0.88 | 2.31 |
| Ozone cleaned | 0.35 | 82.35 | 1.23 | --- | 0.08 | 85.58 | 1.05 | --- | 1.26 | 88.17 | 0.64 | 1.65 | 1.14 | 89.85 | 1.27 | --- |
| Soldermask | | | | | | | | | | | | | | | | |
| As-received | 1.97 | 74.95 | 1.80 | 8.48 | 1.58 | 78.3 | 1.53 | 14.56 | 1.69 | 81.96 | 0.93 | 4.33 | 4.06 | 81.15 | 1.87 | 6.46 |
| Plasma cleaned | 15.47 | 96.36 | 0.49 | 12.39 | 17.00 | 97.79 | 0.42 | 12.41 | 23.78 | 94.78 | 0.25 | 10.05 | 12.06 | 108.06 | 0.51 | 8.02 |
| Ozone cleaned | 1.60 | 80.86 | 0.66 | --- | 3.06 | 82.36 | 0.56 | --- | 8.25 | 80.94 | 0.34 | 8.32 | 2.17 | 88.58 | 0.68 | --- |
| Passivations | | | | | | | | | | | | | | | | |
| SiO ₂ | 17.81 | 90.06 | 0.44 | 21.47 | 20.26 | 90.57 | 0.37 | 6.76 | 28.62 | 85.98 | 0.23 | 21.6 | 15.38 | 100.78 | 0.45 | 19.71 |
| Ozone cleaned SiO ₂ | 6.13 | 84.15 | 0.52 | --- | 8.21 | 85.03 | 0.44 | --- | 15.16 | 81.85 | 0.27 | 14.12 | 5.53 | 93.04 | 0.54 | --- |
| Si ₃ N ₄ | 12.19 | 89.87 | 0.47 | 12.37 | 14.29 | 90.73 | 0.40 | 8.87 | 21.82 | 86.97 | 0.25 | 24.84 | 10.11 | 100.24 | 0.49 | 20.38 |
| Ozone cleaned Si ₃ O ₄ | 11.60 | 87.92 | 0.47 | --- | 13.87 | 88.61 | 0.40 | --- | 21.61 | 84.64 | 0.24 | 15.90 | 9.90 | 97.91 | 0.48 | --- |

γ_{12} (mJ/m²) – Interfacial Tension

W_a (mJ/m²) – Work of Adhesion

ρ - Polarity ratio ($\gamma_{UF}^{Polarity} / \gamma_{SUB}^{Polarity}$)

σ (MPa) - Shear stress

- Technology*, L-H Lee (Ed.), Part A, Plenum Press, New York (1975), pp.129-168.
4. Kim, S., "The role of plastic package adhesion in performance", *IEEE Trans-CHMT*, Vol. 14, No. 4 (1991), pp.809-817.
 5. Wu, S., "Polar and nonpolar interactions in adhesion", *J. Adhesion*, vol. 5 (1973), pp.39-55.
 6. Wu, S., *Polymer Interface and Adhesion*, Marcel Dekker (1982).
 7. Kim, J.K. & Mai, Y.W., *Engineered Interface in Fibre Reinforced Composites*, Elsevier, New York (1998), Chapter 2.
 8. Lu, J., Wu, J., Liew, Y.P., Lim, T.B. & Zong, X., "The impact of underfill properties on theromechanical reliability of flip chip assembly", *Proc. 3rd International Symposium on Electronics Packaging Technology*, Aug. 17-21st 1998, pp.311-316.
 9. Lu, J., Trigg, A., Wu, J. & Chai, T., "Detecting underfill delamination and cracks in flip chip on board assemblies using infrared microscope", *Int. J. Microcir. & Electron. Packag.*, vol. 21. No. 3, 3rd quarter (1998), pp.231-235.
 10. Lau, J., and Chang, C., "Characterization of Underfill Materials for Functional Solder Bumped Flip Chips on Board Applications", *IEEE Trans on CPMT-Part A*, Vol. 22, No. 1 (1999), pp.111-119.
 11. Lau, J., Lee, S.W.R., Chang, C., and Ouyang, C. (1999), "Effects of Underfill Material Properties on the Reliability of Solder Bumped Flip Chip on Board with Imperfect Underfill Encapsulant", *49th Electronic Components and Technology Conference*, San Diego, CA, 1999, pp.571-582.
 12. Wang, J., Lu, M., Zou, D. & Liu, S., "Investigation of interfacial fracture behaviours of a flip-chip package under a constant concentrated load", *IEEE Trans. on CPMT - Part B*, vol. 21, No. 1, Feb. (1998), pp.79-85.
 13. Gamota, D.R. & Melton, C.M., "Encapsulant materials system for flip-chip-on-board assemblies: addressing manufacturing issues", *Circuit World*, 24/1 (1997), pp.7-12.
 14. Kook, S.Y., Snodgrass, J.M., Kirtikar, A. & Danskandt, R.H., "Adhesion and reliability of polymer/inorganic interfaces", *J. Electron. Packag.*, vol. 120, Dec. (1998), pp.328-334.
 15. Jalonen, P. & Tuominen, A., "The importance of solder resist adhesion in flip chip application", *2nd Workshop on Advances in PCB and Substrate Technologies*, Berlin, June 1999.
 16. Tuominen, A., Yamamori, K. & Mugishima, T., "Evaluation of underfills fluxes and solder resists for flip chip applications by single lap shear test", *1999 IEMT/IMC Proc.*, 1999, pp.72-77.
 17. Wertheimer, M.R., Martinu, L., Klembergsaplieha, J.E. & Czeremuskin, G., "Plasma treatment of polymers to improve adhesion", *Adhesion Promotion Techniques*, K.L. Mittal & A. Pizzi (Eds.), Marcel Dekker (1999), Chapter 5.
 18. Lee, C., Gopalakrishnan, R., Nyunt, K., Wong, A., Tan, R.C.E. & Ong, J.W., "Plasma cleaning of plastic ball grid array package", *Microelectront. Reliab.*, 39 (1999), pp.97-105.
 19. Chun, D.S. & Doane, D.A., "Reduction of popcorning in BGA's by plasma cleaning", *2nd Pan Pacific Microelectronics Symposium*, Jan. 1997.
 20. Yi, S., Shen, L., Kim, J.K. & Yue, C.Y., "A failure criterion for bonding between encapsulants and leadframes in plastic IC packages", *J. Adhes. Sci. Technol.*, 14 (2000), pp.93-105.
 21. Yi, S., Kim, J.K., Yue, C.Y. & Hsieh, J.H., "Adhesion strength of epoxy moulding compounds to gold-plated copper leadframes", *J. Adhesion*, 73 (2000), pp.1-17.
 22. Luo, S., Vidal, M. & Wong, C.P., "Surface tension study of substrates in electronic packaging", *2000 Int. Symp. Adv. Packag. Mater.*, 2000, pp.326-331.
 23. Luo, S., Harris, T. & Wong, C.P., "Study on surface tension and adhesion for flip chip package", *2001 Int. Symp. Adv. Packag. Mater.*, 2001, pp.299-304.
 24. Lu, J., Wu, J., Liew, Y.P., Lim, T.B. & Zong, X., "The impact of underfill properties on theromechanical reliability of flip chip asseblly", *Proc. 3rd International Symposium on Electronics Packaging Technology*, Aug. 17-21st 1998, pp.311-316.
 25. Rzepka, S., Korhonen, M.A., Meusel, E., & Li, C.Y., "The Effect of Underfill and Underfill Delamination on the Thermal Stress in Flip-Chip Solder Joints", *J. Electron. Packag.*, Vol. 120, Dec. (1998), pp.342-348.
 26. Sham, M.L. & Kim, J.K., "Effects of flux residue and thermomechanical stresses on delamination failure in flip chip packages", *2000 Inter. Symp. Electron Mater. & Packag. (EMAP2000)*, 2000, pp.274-281.
 27. Viswanadham, P., "Role of adhesion and its reliability implications in electronic assemblies", *4th International Conference on Adhesive Joining and Coating Technology in Electronics Manufacturing*, Espoon, Finland, June 18-21, 2000, pp.28-34.
 28. Park, C.E., Han, B.J., Bair, H.E., and Raju, V.R., "Evaluation Of Epoxy Underfill Materials For Solder Flip-Chip Technology", *J. Mater. Sci. Lett.*, 16 (1997), pp.1027-1029.
 29. Yao, Q., Qu, J., Wu, J. & Wong, C.P., "Characterization of underfill/substrate interfacial toughness enhancement by silane additives", *IEEE Trans. on Electron. Packag. Manuf.*, vol. 22, No. 4, Oct. (1999), pp.264-267.
 30. Dai, X., Brillhart, M.V., Roesch, M. & Ho, P.S., "Adhesion and toughening mechanisms at underfill interfaces for flip-chip-on-organic substrate packaging", *IEEE Trans. Comp. Packag. Technol.*, 23 (2000), pp.117-127.
 31. Bichler, C.H., Langowski, H.C., Moosheimer, U. & Seifert, B., "Adhesion mechanism of aluminium, aluminium oxide and silicon oxide on biaxially oriented polypropylene, PET and PVC", *J. Adhes. Sci. Technol.*, 11 (1997), pp.233-246.
 32. Luo, S. & Wong, C.P., "Surface property of passivation and solder mask for flip chip packaging", *51st Electronic Components and Technology Conference*, 2001, pp.1350-1355.

33. Liston, E.M., "The relationship between water wettability and adhesion bonding", *Polym. Mater. Sci. Eng.*, 62 (1990), pp.423-427.
34. Clouet, F., Shi, M.K., Prat, R., Holl, Y., Marie, P., Leonard, D., De Puydt, Y., Bertrand, P., Dewez, J.L. & Doren A., "Multitechnique study of hezatriacontane surfaces modified by argon and oxygen RF plasmas: effect of treatment time and functionalization, and comparison with HDPE", *Plasma Surface Modification of Polymers*, M. Strobel, C. Lyons and K.L. Mittal (Eds), VSP BV (1994), pp.65-97.
35. Ganesan, G.S., Lewis, G.L. & Berg, H.M., "Contact angles as a measure of interfacial integrity: Theory and experiments", *Adv. In Electron. Packag.*, ASME, EEP-Vol. 10-2, 1995, pp.717-722.
36. Gutowski, W., "Effect of fibre-matrix adhesion on mechanical properties of composites", *Controlled Interphase in Composite Materials*, H. Ishida (Ed.), Elsevier Science (1990), pp.505-520.

The Effect of Melting Time on Lead-free Solder Strength

Kari Määttä¹⁾, Jouko Happonen²⁾ and Aulis Tuominen²⁾

¹⁾ Turku Polytechnic, 24100 Salo, Finland

²⁾ Pori School of Technology and Economics,
Pohjoisranta 11, 28100 Pori, Finland

Abstract

In this test, the effect of melting time on reflow soldering of lead-free solder was investigated. Lead-free solders, which had been qualified in a previous test, were used. The production window for the melting time was investigated. As is known, the melting time for solder joints should not be too short since this may cause cold joints. On the other hand, solder time should not be too long, either, because this may cause brittle intermetallic, weakened solder joints. Also, components cannot withstand too long a period in the elevated temperature needed to melt the lead-free solder.

In the test, samples of copper rod 3 mm in diameter were used and soldered together on their ends. The melting time in the reflow oven was set to be that recommended by manufacturers. The variations in the time were adjusted to be about 30 % shorter than the recommended one and also two times longer as well as about four times longer than recommended. Using a universal pulling test machine, the effect of the melting time on the solder strength was tested. The pulling force needed to break the joint was measured and compared. The strength of a normal tin-lead soldered joint was tested and used as a reference level.

1. Introduction

Soldering is the most important method for joining of mechanical components in electronics. Every component has at least two contacts to be joined.

However, for environmental reasons the traditional solders containing lead have been avoided. Prohibition of lead in solder materials in the European Union will go into effect at the beginning of the year 2008 and will be implemented already by 2006. Nevertheless, few manufacturers have yet implemented lead-free soldering in practice [2] [3].

The traditional tin-lead soldering method has been used a few hundred years, at first in the mechanical joining of components and then, from the beginning of the last century, in electronics where it reliable method.

There are not very many tests made for lead-free solders has been shown to be a very usable and and lead-free soldering is not fully qualified in use.

Pure tin has been used in some coating techniques. However, the melting point of tin is much higher than for eutectic tin-lead solder.

Because of the lack of information regarding reliability in practice, a lot of reliability tests, for instance, thermal cycling and vibration tests, are needed before lead-free solder can replace traditional tin-lead solder.

Testing with a universal tester will show the pulling strength of a joint. In the solder joint, the amount of harmful tin-copper intermetallic increases as a function of temperature and time.

The growth of harmful intermetallic causes brittleness and weakening of the solder joint. The growth of intermetallic is shown in Equation 1 and in Table 1 [1].

$$\delta = k\sqrt{t} \quad (1)$$

where,

δ = thickness of layer [nm]

k = growth factor [nm*s^{-1/2}]

t = time [sec.]

Table 1. Coefficient k [nm * s^{-1/2}]

| Sn -Cu | 20°C | 100°C | 150°C | 170°C |
|--------------------------|------|-------|-------|-------|
| k[nm*s ^{-1/2}] | 0.26 | 1.4 | 3.8 | 10 |

In table 1 we can see the effect of temperature on the growth factor, k. The growth of factor k depends on the formation of metal alloy (Sn-Cu) [1].

2. Test arrangement

In the test, pieces of copper rod 3 mm in diameter and about 25 mm long were soldered together. The ends of the copper rods were smoothed in a lathe to obtain flat and smooth surfaces. The copper surfaces were cleaned with isopropyl alcohol to remove any grease.

The soldering jig used was made from FR-4 PWB material by milling in jig grooves of approx. 2.5 mm in width to accept the samples to be soldered. Soldering paste was applied manually onto the ends of the copper specimens. The grooves on the soldering jig kept the copper rods in position during soldering.

The investigated soldering paste was a lead-free soldering paste (Paste A) which was compared to a soldering paste containing lead (Paste B) and to a paste containing bismuth (Paste C). See Table 2. Table 3 shows melting times, soldering temperatures and speed of the soldering machine for different soldering pastes [4] [5] [6].

Table 2. Tested solder pastes

| Paste sample | [%] | [%] | [%] |
|----------------------------|---------|--------|--------|
| A=(lead-free) | Sn/95.8 | Ag/3.5 | Cu/0.7 |
| B=(tin-lead) | Sn/62 | Pb/36 | Ag/2 |
| C=(lead-free with bismuth) | Sn/58 | Bi/42 | --- |

Table 3. Tested solder pastes. Melting time [s], Temperature [°C] and Speed [mm/min]

| Paste sample | Test 1 | Test 2 | Test 3 | Test 4 |
|-----------------|-----------------|-----------------|------------------|------------------|
| A Tamura | 12/220 /1.07 | 40/220 /0.9 | 80/220 /0.6 | 200/220 /0.35 |
| B Techno Eye | 32/183 /1.0 | 42/183 /0.85 | 122/183 /0.60 | --- |
| C Heraeus | 22/138 /0.9 | 44/138 /0.7 | 100/138 /0.7 | --- |

Temperature profiles for soldering pastes were taken as guide values from specifications of soldering paste manufacturers, which were then modified as shown in the following figures:

- for lead-free Tamura solder (A) Figure 1
- for tin-lead Techno eye solder (B) Figure 2
- for lead-free Heraeus solder (C) Figure 3.

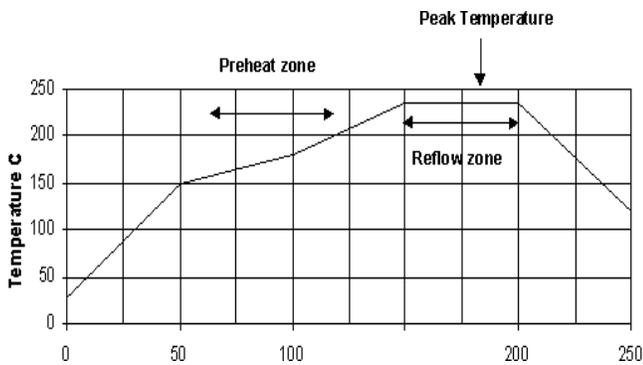


Figure 1. Lead-free solder (Tamura)

Typical Reflow Profile

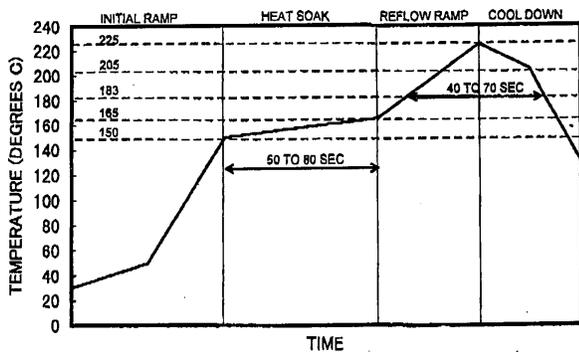


Figure 2. Tin-lead solder (Techno Eye).

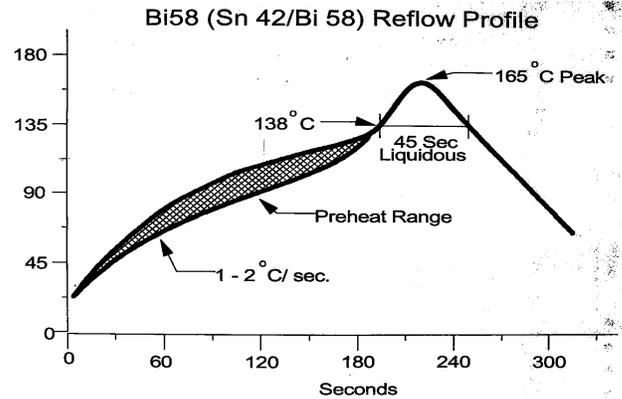


Figure 3. Lead-free solder (Heraeus).

A reflow oven of the type KOKI-UHARC was used in soldering and the pulling test machine was of type Testometric M350-5KN.

Temperature profiles of the reflow oven were set so that the maximum temperature would not go over the adjusted limit value. The melting time was varied by changing throughput time of the oven and temperatures of different zones in the oven. Temperature probes of the test board were set to the same place on the upper side of the test board where soldered samples were placed during the soldering process.

Mechanical strength was tested with the pulling test machine. During the pulling test the samples were pulled at a constant speed of 0.3 mm/min. A computer registered the force used in the test.

The test results of the pulling machine are shown in figures 4a, 4b, 4c and 4d. In these figures, samples (A) were soldered with lead-free solder paste, samples (B) were normal tin-lead solders and samples (C) were soldered with lead-free solder paste containing bismuth. In these tests the melting time was changed as shown in table 3. The pulling force of each sample was measured when the melting time was changed.

3. Results and discussion

Figure 4a shows the pulling strength when the melting time was shortened about 30% - 80% (0.3 times - 0.8 times). Figure 4b shows all results with the melting time of the specifications of the manufacturers (=100%). In Figure 4c the melting time has been lengthened (about 2 times - 3 times) and in Figure 4d only lead-free solder paste was used (melting time was quite long: T = 5 times) [4] [5] [6].

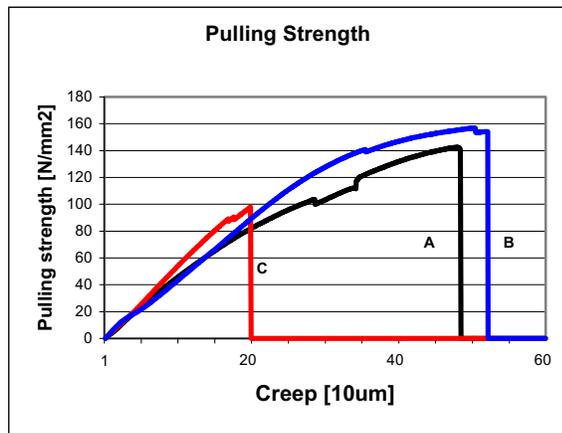


Figure 4a. Shortened melting time

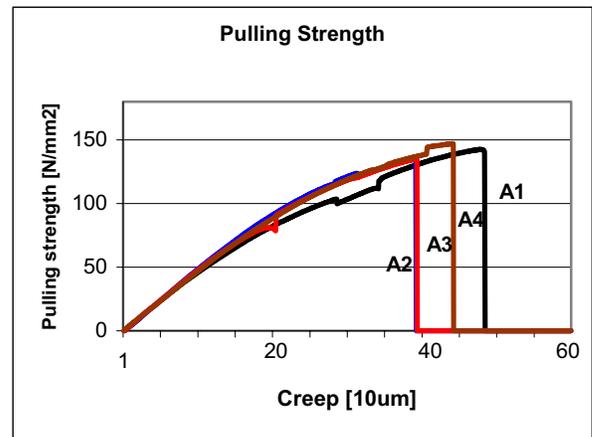


Figure 4d. Lead-free solders. Melting times:
A1 =12s, A2 =40s, A3 =80s, A4 =200s

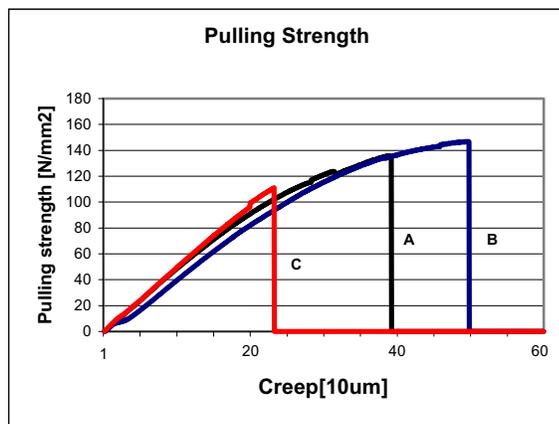


Figure 4b. Normal melting time

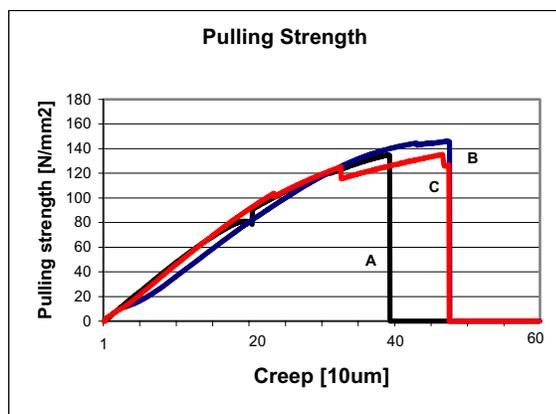


Figure 4c. Lengthened melting time

Table 4 shows, for each of the solder pastes, the maximum pulling breaking strength [N/mm²] with the different melting times [s].

Fluxes of the tin-lead solder pastes may have an effect on strength of the solder joints [7].

The results of the tests show that the differences in the normal and the nearly normal melting times have no great effect on the pulling strength.

With a much longer melting time, when the values of the specifications are exceeded 5 times, the strength of the solder joint is not weakened as expected, but instead, the lengthened melting time seems to increase the durability and the toughness of the solder joint.

Table 4. The pulling strength [N/mm²] and the melting time[s]

| Paste | Melting time 1 | Melting time 2 | Melting time 3 | Melting time 4 |
|-------|----------------|----------------|----------------|----------------|
| A | 143 | 136 | 135 | 147 |
| B | 12 | 40 | 80 | 200 |
| C | 154 | 147 | 146 | — |
| | 32 | 42 | 122 | |
| | 98 | 111 | 127 | — |
| | 22 | 44 | 100 | |

In Figure 4a - 4d the curve is caused by creep mechanism. Creep's mechanism is a permanent, irreversible deformation and it results finally in failure of joints. There are many metallurgical factors affecting the creep rate. The grain size, the degree of prior strain is the most important factors. It has been seen that the creep elongation is also highly dependent on the pressure, by which the specimens were pressed together. Higher stress caused narrower space to be filled by solders, thus allowing shorter elongation before rupture [8].

The maximum shear strengths are shown as bar diagram in Figure 5.

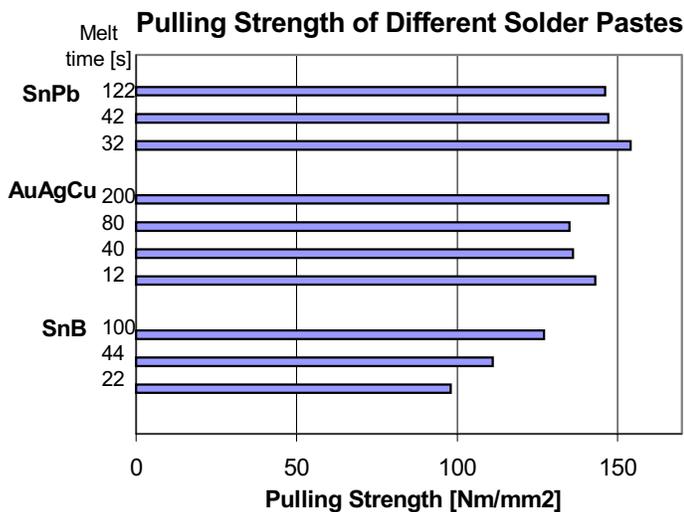


Figure 5. Shear strength of different solderpastes [N/mm²]

4. Conclusion

The tests seemed to show that, contrary to what was assumed, an extended melting time improved soldered joint reliability.

This means that a moderately longer melting time didn't produce a harmful amount of Sn₆Cu₆ intermetallic layer. The extended melting time seemed to increase the durability and the toughness of the soldered joint.

Table 4 shows the average value of the pulling strength tests at the breakdown points for all types of solder paste (sample types A, B and C). The results are also presented graphically in figures 4a, 4b, 4c and 4d.

The lead-free solder paste used in the tests proved usable although the melting time was extended three times beyond the normal. It should also be noted, that the extension of the melting time of the solder will increase the stress to the soldered components. Also, the temperatures used in lead-free soldering are a bit higher, and this causes an extra stress to the components. It is uncertain what will happen when lead-free solder joints are temperature cycled.

The lead-free solder paste will have to be tested with all traditional test methods like vibration, heat cycling and other burden tests, before it is possible to replace the traditional tin-lead solder with lead-free solder paste in the entire production.

However, it is well to keep in mind that at present, the temperature cycling test is very rigorous compared to the stress encountered during the whole lifetime of a lead-free soldered product [9].

Acknowledgements

The authors would like to thank Mr. Kauko Peltonen for helping us to arrange samples and Mr. Rami Järvenpää for performing the pulling tests.

5. References

1. Wassink, R. J. K., Soldering in Electronics, Electrochemical Publications Ltd., Ayr, Scotland, 1989, p. 149-158, p. 187.
2. Turunen, J., Kinnunen, M., Lyijyttömät prosessit. Elektroniikan tuotantotekniikan pk-harjoitustyö. Elektroniikan laitos. LTKK 6.10.2000
3. Larvikko, P., Nurmi, S., Alander, T., Nykänen, J., Pienimaa, S., Ristolainen, E., Lyijytön juote Haaste ja mahdollisuus. ETX-tutkimusohjelma. www.proessori.fi/es99/unleaded.htm.
4. Specification of Tamura soldering paste (Paste A).
5. Specification of Hereaus soldering paste (Paste B).
6. Specification of Techno Eye soldering paste (Paste C).
7. Happonen, J., Maattanen, K., Tuominen, A., "Evolving Flip Chip Fluxes", Future EMS International, Issue 1, Technology Publishing Ltd, 1999, pp. 115-118.
8. Muukkonen, E., Pirttikoski, P., Tuominen, A., "Characterization of Creep Phenomena in a Flux Junction between the IC-Device and a Copper Plated Printed Circuit Board", 6th IMAPS Nordic Annual Conference in Helsinki, Finland, 19-23 September 1999.
9. Maattanen, K., Happonen, J., Tuominen, A., "Segregation Of Tin Lead Structures In Old Solder in Sem Analysis Vs., Temperature Cycling", 3rd IEMT/IMC Symposium, Omiya, Japan, 1999, pp. 298-303.

Intermetallic Growth between Sn-Ag-(Cu) solder and Ni

Seung Taek Yang, Yoon Chung and Young-Ho Kim

Dept. of Materials Engineering, Hanyang Univ. Seoul, 133-791, KOREA

B. H. Hong, and K. R. Park

Amkor Technology Korea, Inc. Korea

H. G. Song and J. W. Moris, Jr

U. C. Berkeley, CA, USA

E-mail : yox6648@daum.net, Phone : 82-2-2290-0405, Fax : 82-2-2293-7445

Abstract

The intermetallic formation between Sn-Ag-(Cu) solders and metal pads was characterized using scanning electron microscopy(SEM), Energy Dispersive Spectroscopy(EDS), and X-ray Diffractometer(XRD). The intermetallic phase formed in the interface between Sn-Ag-Cu and Au/Ni/Cu pad in tape BGA package is likely to be ternary compound of Cu-Ni-Sn from EDS analysis. Cu was also segregated in the solder/Ni interface. XRD analysis confirmed that η -Cu₆Sn₅ type intermetallic phase formed in the interface between Cu containing solders and Ni substrates and Ni₃Sn₄ intermetallic formed in the Sn-Ag solder/Ni interface. The Cu atoms in the solder seem to diffuse in the solder/Ni interface and to form Cu₆Sn₅ type intermetallic in the Sn-Ag-Cu specimens. The increase in the Cu concentration of the solder increased the intermetallic thickness after reflow.

Introduction

The tin-lead solder alloys have been widely used in the electronic industry, because of its abundant nature storage, low cost, suitable melting point, and excellent soldering properties. However, because lead and lead compounds are poisonous, the usage of them will not only bring the environmental pollution but also will impair worker's health. Nowadays many governments tend to forbid the usage of lead-containing products[1]. Many electronic manufacturers have announced their road maps to replace Pb-containing solder connections with Pb-free solder ones. In US, several Pb-free programs have been initiated by several professional societies, in order to integrate the industry-wide efforts to implement Pb-free solutions in a timely fashion[2]. The new solder must be able to produce solder joints with acceptable joint strength, and at the same time, also be able to withstand thermal fatigue over the projected operating life of the soldered assembly and meet other reliability requirements, such as adequate corrosion, oxidation and electromigration resistance. The material cost of a new solder should not be so high as to overwhelm the assembly cost. With the above guidelines in mind, a number of Pb-free solders have newly been developed. Some of the examples include Sn-3.5%Ag, Sn-3.5%Ag-0.7%Cu, Sn-3.5%Ag-4.8%Bi, Sn-0.7%Cu, Sn-5%Sb, Sn-20%In-3%Ag, Sn-8%Zn-3%Bi and Sn-10%In-3%Ag-1%Cu[2]. Sn-Ag solders with small addition of Cu is considered as one of the best solders which replace eutectic Pb-Sn solder because of its advantages in reliability, mechanical properties and solderability compared with other lead-free alternatives such as above solders.

The reliability of the solder joints is sensitive to the type and the thickness of intermetallic phase. The composition of intermetallic is dependent primarily on the solder composition[3]. The formation of intermetallic compound(IMC) layer provides a chemical bonding between the solder and the substrate and is necessary for the joint strength, but an overgrown IMC layer is known to be detrimental to the joint strength due to the brittle nature of IMCs. The Sn-3.5Ag-0.7Cu solder bumps on Ni have interfacial intermetallics with Ni-Cu-Sn ternary composition and the Sn-3.5Ag-0.7Cu solder bumps on Cu have Cu₆Sn₅. It is widely reported that the Sn-3.5Ag solder without Cu forms a binary compound Ni₃Sn₄[2-6]. Kang reported that the intermetallic compounds grown in Sn-Ag-Cu appeared to be of two layers, which consist of the top layer having a higher Cu contents than Ni and the bottom layer attached to the Ni layer having a higher Ni content than Cu[7]. The Sn-3.5Ag-0.7Cu solder bumps on Ni characterized intermetallics of Ni-Cu-Sn ternary compositions as (Ni, Cu)₆Sn₅ intermetallics from EDS analysis[4]. In the present investigation, the intermetallic phases were analyzed using XRD as well as SEM and EDS. In addition, we investigated the effects of Cu concentration in Sn-Ag solders on the morphology and the growth of intermetallics.

Experimental Procedure

Two types of specimens were used in the present study. The 1st type specimen was the real BGA sample(FlexBGA[®] by Amkor Technology). The Sn-4.0wt%Ag-0.5wt%Cu or Sn-3.5wt%Ag solder balls were placed on the Au(max1.0 μm)/Ni(1.5 μm)/Cu(18 μm) pads and the solder bumps were formed after reflowing at 240 °C. The second type specimen was fabricated specially for XRD analysis. The Sn-4.0wt%Ag-0.5wt%Cu or Sn-3.5wt%Ag solder balls were mounted on Ni foil with the flux and reflow at 240 °C. Also, the intermetallic formation was characterized in the interfaces between Sn-Ag-Cu solders with various Cu contents and Ni foils.

The both type specimens were mounted with epoxy and were metallographically prepared to a final finish of 0.05 μm alumina slurry for SEM analysis. EDS analysis was also performed to determine the elemental compositions of intermetallic phases quantitatively. XRD specimens were made by etching out the solders in a 10%HNO₃+90%H₂O solution so that the IMC structure was fully exposed(Fig. 1).

Result and Discussion



Fig.1. Etching of solders for SEM and XRD analyses.

Sn-Ag-(Cu) solder balls / UBM(Au/Ni/Cu)

Fig. 2 shows the cross-sectional optical image of solder bumps on Au/Ni/Cu UBM. Solder bumps on Ni/Cu UBM pads are clearly seen. Since the thin Au layer is dissolved into the solder, the Ni layer became in contact with the Sn-Ag-(Cu) solder. Intermetallic is formed between Sn-Ag-(Cu) solder and Ni layer. Fig. 3 and 4 show the cross-sectional SEM images of Pb-free solder bumps on Au/Ni/Cu. These samples were reflowed once or five times. Two types of intermetallics were observed; one was observed between the solder/UBM interface and the other was observed in the bulk solder. In the bulk solder, large intermetallic particles such as Ag_3Sn formed. Interfacial intermetallics of dendrite-type were observed in the interface between Sn-Ag-Cu solder and Au/Ni/Cu UBM, on the other hand blocky type intermetallics



Fig. 2. FlexBGA®.

were observed between Sn-Ag solders and the UBM. The thickness of interfacial intermetallic increased after the 5th reflow. The composition of the intermetallic found in the interface between Sn-Ag-Cu solder and Au/NiCu UBM was analyzed using EDS technique; Ni, Cu and Sn have 22, 33, 45 at% respectively. These EDS analysis indicates that the intermetallic is likely to be $(\text{Cu}, \text{Ni})_6\text{Sn}_5$. After removing the solder by 10% HNO_3 +90% H_2O solution, intermetallic morphology was observed by SEM(Fig. 5 and 6). In Fig. 5, thin needle-like intermetallics were observed and each needle-like feature thickened after 5th reflow. Fig. 6 shows the morphology of the intermetallics were needle-like after the 1st reflow and become more square after the 5th reflow. Comparison of the morphology of the intermetallic phase(Fig. 5 and Fig. 6) tells the intermetallic phase formed in the Sn-

Ag-Cu solder is different that in the Sn-Ag solder. Fig 5 and Fig. 6 also show one column of intermetallic thickened with the number of reflows. Fig. 7 and Fig.8 show the elemental X-ray mapping results near the interface between the Sn-Ag-

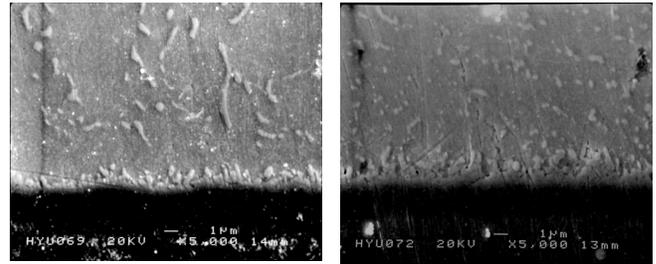


Fig. 3. Cross - sectional SEM images of Sn-4.0wt%Ag-0.5wt%Cu solder bumps on Au/Ni/Cu pads (a) The 1st reflow (b) The 5th reflow.

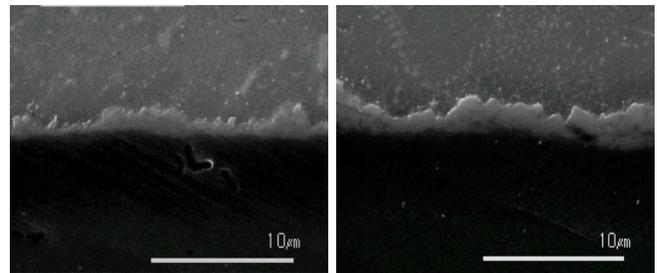


Fig. 4. Cross - sectional SEM images of Sn-3.5wt%Ag solder bumps on Au/Ni/Cu pads (a) The 1st reflow (c) The 5th reflow.

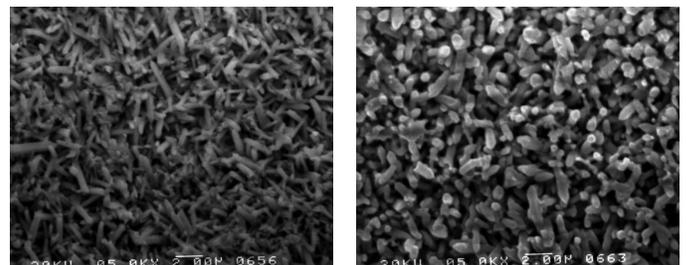


Fig. 5. SEM images showing intermetallic morphologies after Sn-4.0wt%Ag-0.5wt%Cu solder bumps on Ni/Cu UBM pads are etched away layer (a) The 1st reflow (b) The 5th reflow.

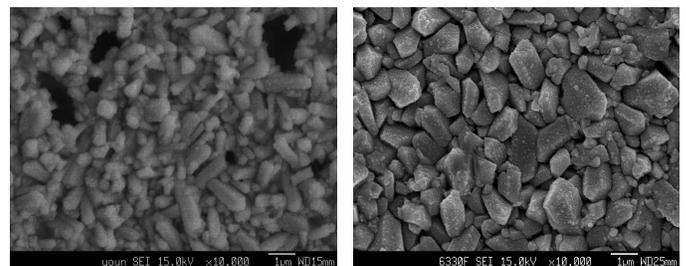


Fig. 6. SEM images showing intermetallic morphologies after Sn-3.5wt%Ag solder bumps on Ni/Cu UBM pads are etched away layer (a) The 1st reflow (b) The 5th reflow.

(Cu) solder and Au/Ni/Cu pads after the 1st and 5th reflows. X-ray mapping results show that Ni was found only on the Ni layer of the metal pad and Ag was found inside the solder. Ag came from Ag_3Sn intermetallics. Cu signal was detected on the top region of Ni layer as well as in the Cu layer below Ni layer. Cu intensity on the top of Ni layer increased after the 5th reflow(Fig. 8).

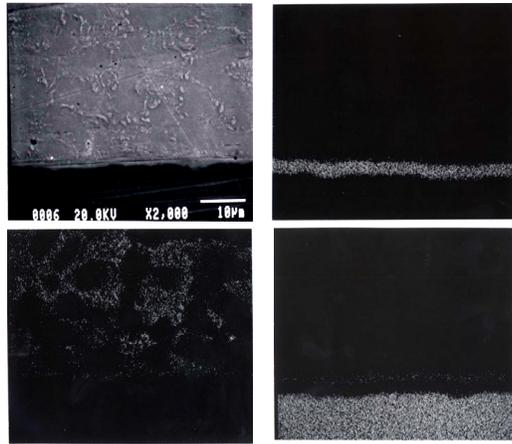


Fig. 7. X-ray mapping of the Sn-4.0wt%Ag-0.5wt%Cu solder bump on Au/Ni/Cu after the 1st reflow.

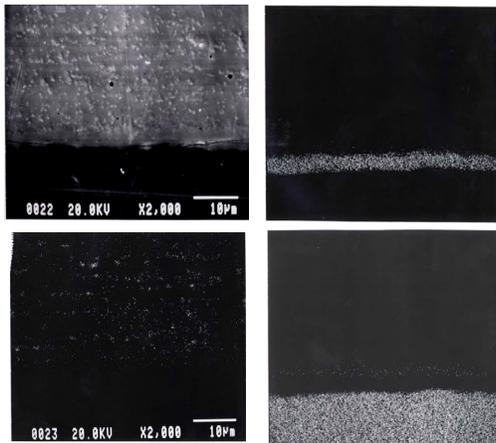


Fig. 8. X-ray mapping of the Sn-4.0wt%Ag-0.5wt%Cu solder bump on Au/Ni/Cu after the 5th reflow.

Sn-Ag-(Cu) solder balls / Ni foil

The intermetallic phase identification by XRD technique was tried in the FlexBGA[®] specimens, but it was difficult because the area of intermetallic formation was too small to get the sufficient intensity. Therefore, we tried for XRD analysis using the specimen where solder balls were placed on the Ni foil and reflowed(Fig 11). Fig. 12 and Fig. 13 show that the intermetallic formed at the solder/Ni interface. The thickness of the intermetallic phase increased with the number of reflows. Fig. 14 shows the XRD patterns of the intermetallics formed on the solder /Ni interface after the 5th reflow. Fig. 14(a) shows that intermetallic compounds

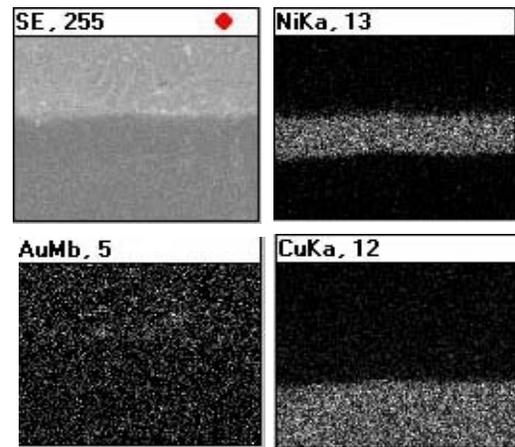


Fig. 9. X-ray mapping of the Sn-3.5wt%Ag solder bump on Au/Ni/Cu after the 1st reflow.

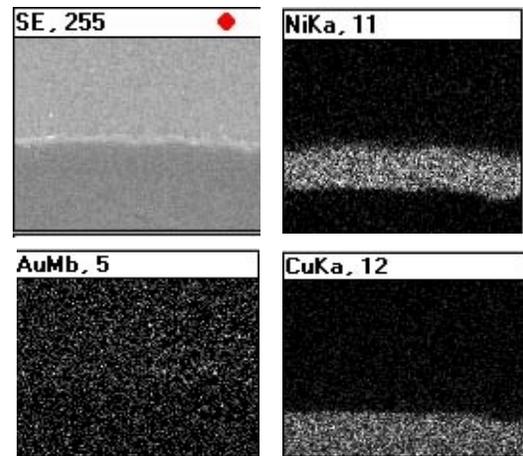


Fig. 10. X-ray mapping of the Sn-3.5wt%Ag solder bump on Au/Ni/Cu after the 5th reflow

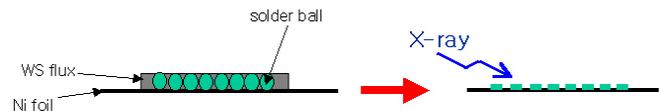


Fig. 11. solder bumps on Ni foil for XRD analysis

observed are Ag_3Sn , Ni_3Sn_4 and Cu_6Sn_5 . Especially, Cu_6Sn_5 phase formation is clearly seen. There is a possibility of Sn and Ni reaction to form Ni_3Sn_4 but additional experiments are necessary to clarify it. In Fig. 14(b), Ni_3Sn_4 and Ag_3Sn were observed. Ni_3Sn_4 observation by XRD confirmed the previous result[2-6]. Table 1 summarized the thickness of intermetallic measured from the cross-sectional SEM images. The results show that intermetallics thickness was increased with the number of the reflow cycles. The intermetallic thickness in the BGA specimen where solder bumps formed on Au/Ni/Cu UBM pad was larger than that in the specimen where solder balls mounted on Ni foil at the same condition. This results seems to be related to the size of metal layer. The intermetallic formation is limited due to the UBM pad size in

the BGA specimen, where as the intermetallic will form on the whole Ni layer in the Ni foil.

Table 1. Summary of intermetallic thickness between solder and metal pad

| specimen | 1st reflow | 3rd reflow | 5th reflow |
|--------------------|--------------------|--------------------|--------------------|
| Sn-Ag-Cu/metal pad | 0.89 μm | 0.94 μm | 1.33 μm |
| Sn-Ag-Cu/Ni foil | 0.47 μm | - | 0.99 μm |
| Sn-Ag/metal pad | 0.70 μm | 1.03 μm | 1.66 μm |
| Sn-Ag/Ni foil | 0.46 μm | - | 0.75 μm |

- : not measured

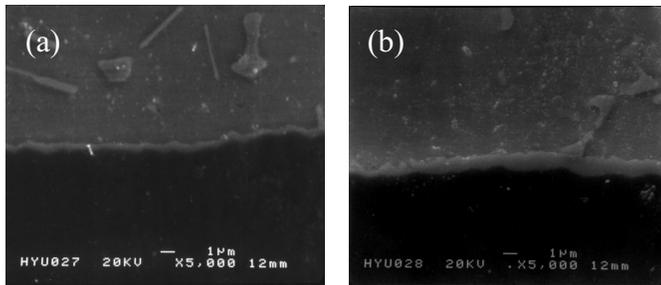


Fig. 12. Cross - sectional SEM images of Sn-4.0wt%Ag-0.5wt%Cu solder bumps on Ni foil (a) The 1st reflow (c) 5th reflow.

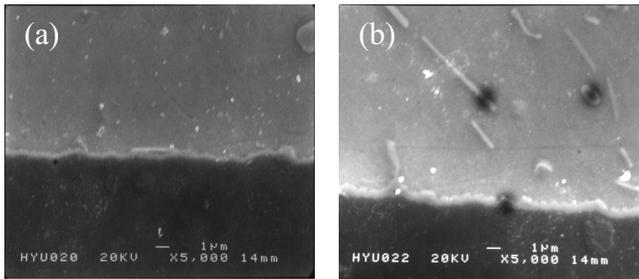


Fig. 13. Cross - sectional SEM images of Sn-3.5wt%Ag solder bumps on Ni foil (a) The 1st reflow (c) The 5th reflow.

Cu segregation was also found in the interface between Sn-4%Ag-0.5%Cu and Ni foil (Fig. 15 and Fig. 16). In these specimens Cu was not contained in the substrate. And Cu segregation was not detected in the interface between Sn-3.5%Ag and Au/Ni/Cu (Fig 9 and Fig. 10). As a result, the Cu contained in the solder was the source of the Cu segregation in the interface. Cu segregation resulted from the formation of the Cu_6Sn_5 type intermetallic phase. It is very interesting that Cu_6Sn_5 type IMC formed at the solder/Ni interface. Many previous studies [1, 4-5] proved that Cu_6Sn_5 growth was very fast during reflow in Pb-Sn solder/Cu joint; specially, faster than Ni_3Sn_4 . Anomalously high diffusion rate of Cu in Sn has

been observed at temperatures below the melting point of Sn [7]. Apparently Cu atoms have a high mobility in liquid Sn, and $(\text{Cu}, \text{Ni})_6\text{Sn}_5$ can grow significantly faster than Ni_3Sn_4 .

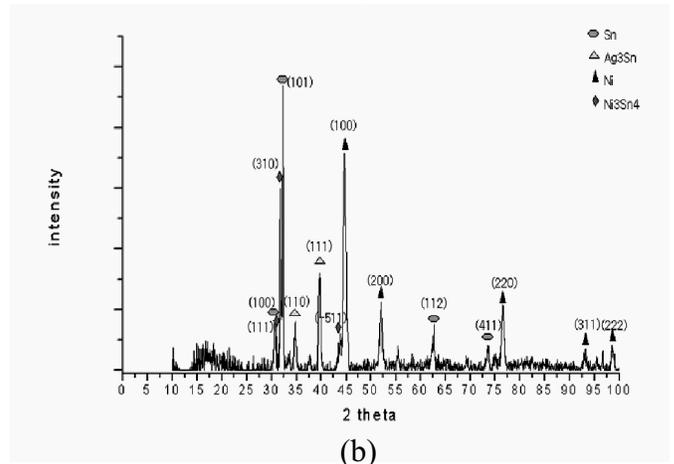
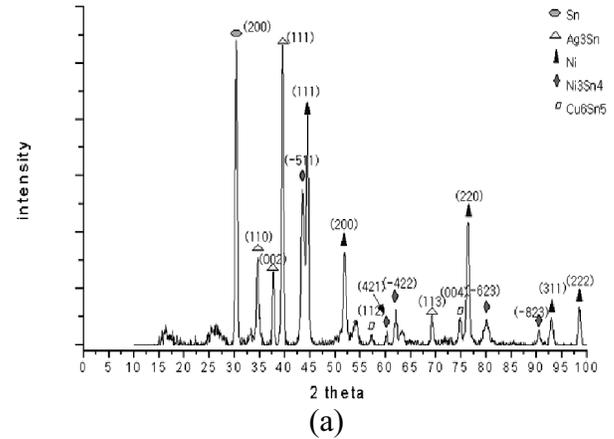


Fig. 14. The XRD patterns of the interfaces in the solder/substrate joints after the 5th reflow. (a) Sn-4.0wt%Ag-0.5wt%Cu solder/Ni foil (b) Sn-3.5wt%Ag solder/Ni foil.

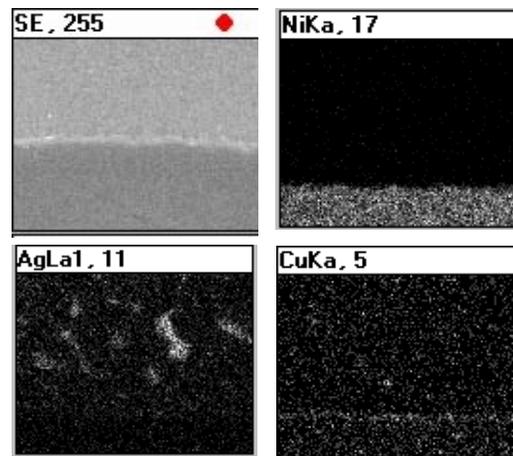


Fig. 15. X-ray mapping of the Sn-4.0wt%Ag-0.5wt%Cu solder bump on Ni layer after the 1st reflow.

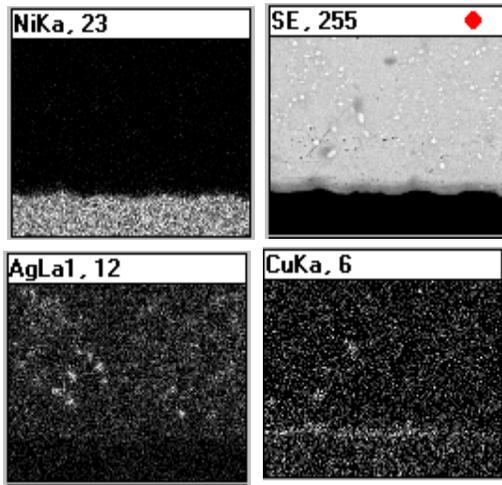


Fig. 16. X-ray mapping of the Sn-3.5wt%Ag solder bump on Ni layer after the 5th reflow.

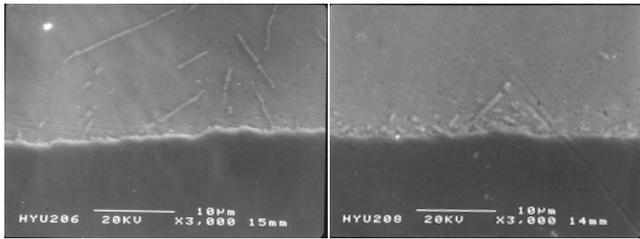


Fig.18. Cross - sectional SEM images of Sn-Ag-0.5wt%Cu solder bumps on Ni foil (a) The 1st reflow (b) The 5th reflow.

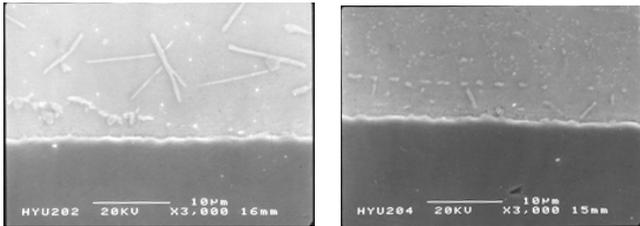


Fig.17. Cross - sectional SEM images of Sn-Ag-0.36wt%Cu solder bumps on Ni foil (a) The 1st reflow (b) The 5th reflow.

The cross-sectional SEM images showing the intermetallic growth on the Sn-Ag-Cu solder with different Cu concentrations(0.36, 0.50, 0.75 and 1.06 wt%) are shown on Fig. 17-Fig. 20. The intermetallic growth behavior in the Sn-Ag solders with various Cu concentrations are summarized in Fig. 21 by plotting the intermetallic thickness with Cu concentration measured from Fig. 17-Fig. 20. The intermetallic thickness increased with Cu concentrations and the number of reflow cycles. The Cu atoms in the solder played a major role to form the intermetallics.

Conclusions

From this investigation following conclusions can be drawn:

1. $(\text{CuNi})_6\text{Sn}_5$ intermetallic was observed in the interface between the Sn-Ag-Cu solder and Au/Ni/Cu UBM in the real BGA specimens. Ni_3Sn_4 intermetallic was observed in the interface between Sn-Ag solder and Au/Ni/Cu UBM. Ag_3Sn intermetallic was observed in Sn-Ag-(Cu) bulk solder.
2. XRD patterns show that η - Cu_6Sn_5 and Ni_3Sn_4 were formed in the interface between Sn-Ag-Cu solder and Ni foil.
3. The Cu contained in the solder was the source of the Cu segregation in the interface.
4. The intermetallic thickness increased with Cu concentration and the number of reflow cycles in the Sn-Ag-Cu solders.

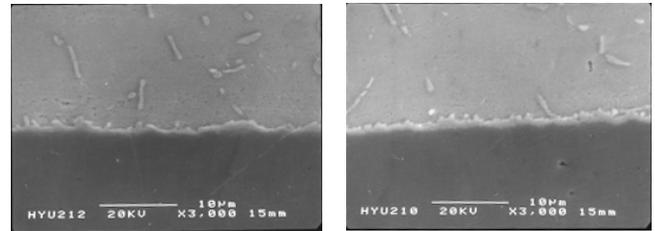


Fig.19. Cross - sectional SEM images of Sn-Ag-0.75wt%Cu solder bumps on Ni foil (a) The 1st reflow (b) The 5th reflow.

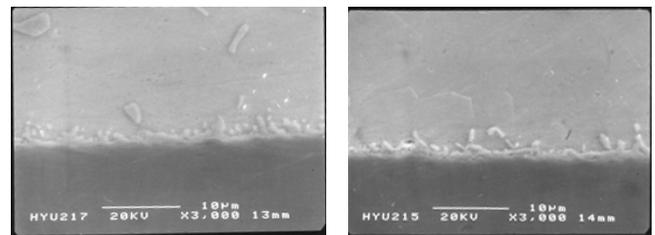


Fig.20. Cross - sectional SEM images of Sn-Ag-1.06wt%Cu solder bumps on Ni foil (a) The 1st reflow (b) The 5th reflow.

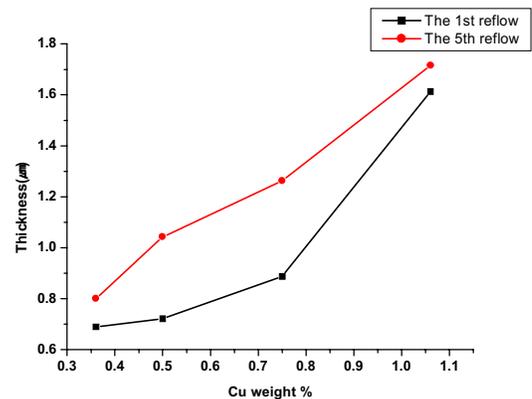


Fig. 21. Intermetallic growth in Sn-Ag-Cu solders with Cu concentration.

Acknowledgments

This work was financially supported by International Joint Research and Development Project. We are grateful to Dr. K. T. Hong for helping in the SEM analysis and examination.

References

- 1 Huang Le, Wang Qian, Ma jusheng, “*The study on Novel Lead-Free Solder Alloy*” 2000 Int’I Symp on Electronic Materials & Packaging, pp 191-193
2. Won Kyoung Choi and Hyuck Mo Lee, “*Interfacial Reaction of Sn-3.5wt%Ag Solder Alloy With a Variance of Ni Layer Thickness*” J. Kor. Inst. Met. & Mater. Vol. 37, No.11(1999), PP 1416-1421
3. C. M. Liu, C. E. Ho, W. T. Chen, C. R. Kao “ *Reflow Soldering and Isothermal Solid-state Aging of Sn-Ag Eutectic Solder on Au/Ni Surface Finish*”
4. K. Zeng, V. Vuorinen, and J. K. Kivilahti, “*Intermetallic Reaction Between Lead-Free SnAgCu Solder and Ni(P)/Au Surface Finish on PWBs*” 2001 Electronic Components and Technology Conference, pp. 693-698
- 5 Chang-keun shin and Joo-Youl Huh, “*Effect of Cu-containing solders on the critical IMC thickness for the shear strngth of BGA solder joints*” 2000 Electronics packaging Technology Conference.
6. Dae-Woong Kang and Joo-Youl Huh, “*Effects of Cu-additions on the Reaction Kinetics Between Sn-Based Solders and Cu substrate*” J. Kor. Inst. Met. & Mater. Vol. 38, No.1(2000), PP 180-186
7. S. K. Kang, D. Y. Shih, K. Fogel, P. Lauro, M. J. Yim et al, “*Interfacial Reaction Studies on Lead(Pb)-Free Solder Alloys*” 2001 Electronic Components and Technology Conference, pp. 448-454
8. B.Salam, N. N. Ekere, D. Rajkumar, “ *Stydy of interface Microstructure of Sn-Ag-Cu Lead-Free Solders and the Effect of Solder Volume on Intermetallic Layer Formation*” 2001 Electronic Components and Technology Conference, pp.471-477
- 9 Jong-Kai Lin, Ananda De Silva, Darrel Frear, Yifan Guo et al. “*Characterization of Lead-Free Solders and Under Bump Metallurges for Flip-Chip package*” 2001 Electronic Components and Technology Conference, pp.455-462
10. A. Zribi, L. Zavalij, P. Borgesen, A Primavera, G. Westby, E. J. Cotts “ *The Kinetics of Formation of Ternary Intermetallic Alloys in Pb-Sn and Cu-Ag-Sn Pb-free Electronic Joints*” 2001 Electronic Components and Technology Conference, pp.687-692

Effect of Heat Treatment on the Interfacial Adhesion Strength between Sn-Zn-xAg Lead-free Solders and Cu Substrate

Tao-Chih Chang¹, Min-Hsiung Hon¹, Chin-Hui Chang², and Moo-Chin Wang²
1 Department of Materials Science and Engineering, National Cheng Kung University

1 Ta-Hsueh Road, Tainan, 70101, Taiwan

2 Department of Mechanical Engineering, National Kaohsiung University of Applied Science
415 Chien-Kung Road, Kaohsiung, 80782, Taiwan

e-mail: n5889114@ccmail.ncku.edu.tw

Phone: 886-6-2757575-62969

Abstract

Sn-9Zn eutectic solder alloy is a potential candidate to replace 63Sn-37Pb alloy as interconnecting material in electronic packaging industry. But the inferior wettability and poor oxidation resistance make this alloy not suitable for application widely.

In this study, different Ag contents were added into the Sn-9Zn alloy to improve the wettability, oxidation resistance, and adhesion strength of interface.

A pull-off test was used to estimate the adhesion strength of interface between Sn-Zn-xAg solders and Cu substrate, scanning electron microscope (SEM) was utilized to observe the fracture morphology, energy dispersive spectrum (EDS) was employed to analyze the distribution of elements. Finally, X-ray diffraction (XRD) was exploited to identify the intermetallic compounds (IMCs) formed at the interface.

Experimental Procedure

The Sn-Zn-xAg lead-free solders used in this study were made with pure metals, and the Ag content x of 0.5, 1.5, 2.5 and 3.5 wt%. Pure Sn, Zn and Ag were mixed in a stainless steel crucible and melted at 600 °C, stirred to homogenization.

Cu substrate (oxygen-free, high conductivity) was degreased in 5 wt% NaOH solution at 70 °C, then rinsed in de-ion water. After degreasing, it was immersed in 5 vol% HCl solution to remove the oxide on the Cu substrate, and rinsed in de-ion water again. After fluxing (flux used in this study was 3.5 wt% dimethylammonium chloride), Cu substrate was dipped in the melted solder alloy as shown in Fig. 1¹, For an excellent wettability, the dipping temperature was controlled at 350±5 °C, for 30 s, at a dipping rate of 11.8 mm/s.

After dipping, the specimens were heat treated at 150 °C for 100, 250, 400, 750 and 1000 hrs, respectively. XRD was utilized to identify the IMCs formed at the interface at a scanning rate of 4 °/s, from 20 to 100 ° of 2 θ . A pull-off instrument² as shown in Fig. 2 was employed to estimate the adhesion strength of interface after heat treatment.

Finally, the fracture morphology was observed with SEM, and EDS was exploited to analyze the distribution of elements.

Surface morphology observation

One of the disadvantages of Sn-9Zn alloy was inferior wettability³⁻⁵, which can be improved by using suitable flux⁶⁻⁷. The flux used in this study was DMAHCl, Fig. 3 shows the smooth morphologies of Cu substrate as dipped in solders. With increasing the silver content in alloy, some unmelted

solder lumps were found on the surface, which were suggested to be high melting point IMCs. The DMAHCl was a very suitable flux for Sn-9Zn system.

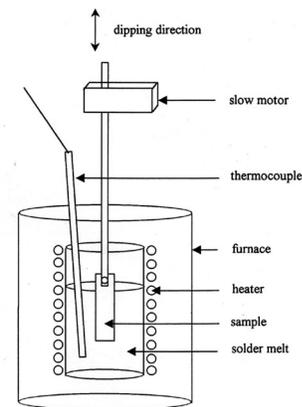


Fig. 1. Dipping apparatus used in this study.

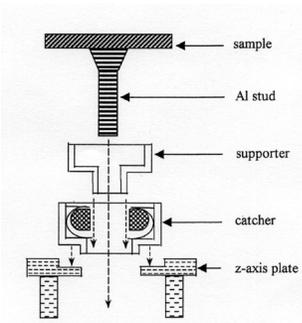
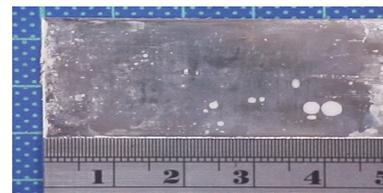
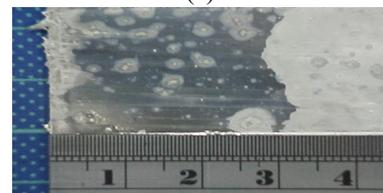


Fig. 2. Schematic diagram of pull-off test instrument.



(a)



(b)

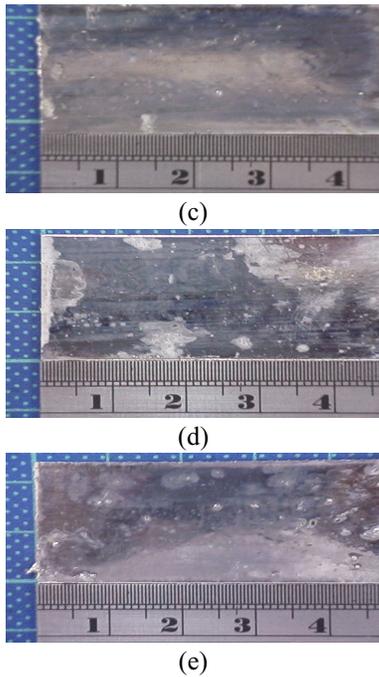


Fig. 3. Surface morphologies of Cu substrate dipped in Sn-Zn-xAg lead-free solders at 350 °C for (a)0.0Ag, (b)0.5Ag, (c)1.5Ag, (d)2.5Ag, (e)3.5Ag

XRD diffraction analysis

XRD patterns were utilized to identify the IMCs formed at the interface between solder and Cu substrate as shown in Figs. 4 and 5. It was found that Cu_6Sn_5 and Cu_5Zn_8 formed at the interface, as the silver content was below 0.5 wt%. When the silver content in solder was above 1.5 wt%, Ag_3Sn IMC was also found at the interface. After heat treatment, it was even found that Ag_3Sn grew as a film on the surface.

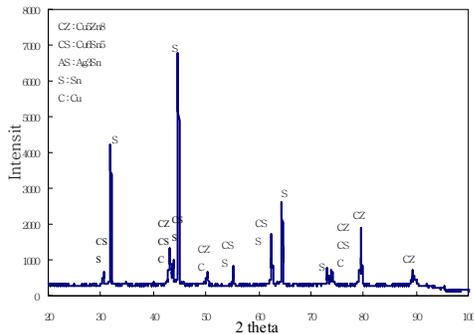


Fig. 4 XRD diffraction pattern of interface between Cu and Sn-Zn-0.5Ag solder after heat-treated at 350 °C for 1000 hrs.

Adhesion strength of interface

Fig. 6 shows the adhesion strength of interface between Cu substrate and Sn-Zn-xAg lead-free solders as dipped at 350 °C for 30 s. It was found that the interface had a maximum adhesion strength of 10.46 MPa when the Ag content was 1.5 wt%. When the Ag content was increased to 2.5 wt%, the adhesion strength of interface decreased to 8.49 MPa. It was suggested that the interfacial bonding was fairly weak between Cu_6Sn_5 and Sn-Ag matrix⁸ decreased the adhesion strength when the Ag content was above 1.5 wt%.

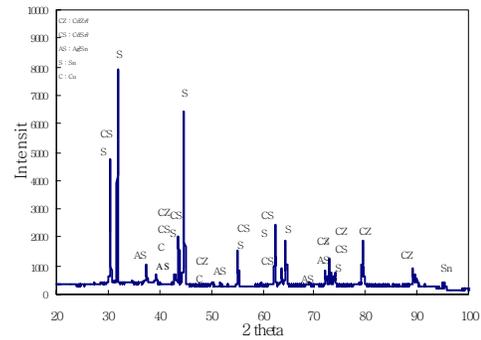


Fig. 5 XRD diffraction pattern of interface between Cu and Sn-Zn-1.5Ag solder after heat-treated at 350 °C for 1000 hrs.

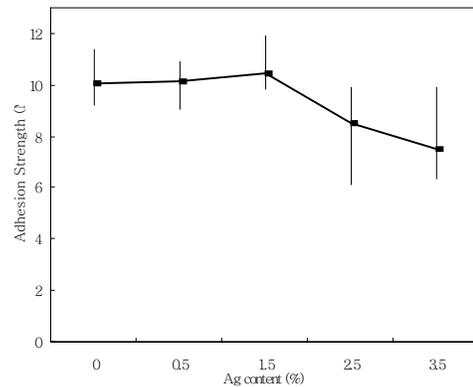


Fig. 6 Adhesion strength of interface between Cu substrate and Sn-Zn-xAg lead-free solders as dipped at 350 °C for 30 s.

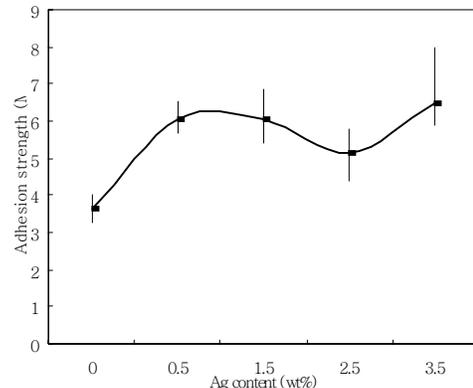


Fig. 7 Adhesion strength of interface between Cu substrate and Sn-Zn-xAg solders after heat-treated at 150 °C for 1000 hrs.

Fig. 7 shows the adhesion strength of interface between Cu substrate and Sn-Zn-xAg lead-free solders after heat-treated at 150 °C for 1000 hrs. It was found that the adhesion strength of interface between Cu and Sn-9Zn alloy decreased from 10.08 to 3.63 MPa as aged. However, adhesion strength of interface between Cu and Sn-Zn-xAg solder decreased from 10.1 to 6.08 MPa only.

Therefore, it was concluded that adding Ag into Sn-9Zn alloy could enhance the heat-resistant property of interface. It was suggested that Ag_3Sn which was formed at interface after heat treatment has excellent adhesion with substrate⁹

Acknowledgement

The authors wish to thank National Science Council of Taiwan for the financial support (NSC89-2216-E-151-011).

Reference

1. S. P. Yu, M. H. Hon, and M. C. Wang, *J. Elec. Mater.*, Vol. 29, No. 2 (2000), pp. 237-243.
2. S. P. Yu, M. C. Wang and M. H. Hon, *J. Mater. Res.*, Vol. 16, No. 1 (2001), pp. 76-82.
3. M. McCormack, S. Jin, *JOM*, July, 1993, pp. 36-40.
4. M. McCormack, S. Jin, *J. Elec. Mater.* Vol. 23, No. 7 (1994), pp. 635-640.
5. E. P. Wood, K. L. Nimmo, *J. Elec. Mater.*, Vol. 23, No. 8 (1994), pp. 709-713.
6. S. Vaynman, M. E. Fine, *Scripta Materialia*, Vol. 41, No. 12 (1999), pp. 1269-1271.
7. M. E. Loomans, S. Vaynman, G. Ghosh, M. E. Fine, *J. Elec. Mater.*, Vol. 23, (1997), p. 741.
8. J. P. Lucas, A. W. Gibson, K. N. Subramanian, T. R. Bieler, *Proc. MRS Spring Meeting, 522* (Warrendale, PA: MRS, 1998), p. 339.
9. K. Suganuma, Y. Nakamura, *J. Jpn. Inst. Metals*, Vol. 59 (1995), pp. 1299-1305.

Creep Deformation of Microstructurally Stable Sn-3.5Ag-xBi solders

S. W. Shin and Jin Yu

Center for Electronic Packaging Materials, KAIST
373-1 Kusong-dong, Yusong-gu, Daejeon, Korea
e-mail) swshin@kaist.ac.kr, jinyu@kaist.ac.kr

Abstract

In the electronics industry worldwide, using lead-free solders is becoming more mandatory recently. On that regard, substantial amounts of work related to lead free solders are under way, and Sn-3.5Ag based ternary alloys with Bi or Cu are strong candidate materials. In the present work, Sn-3.5Ag-xBi alloys with five different levels of Bi (0, 2.5, 4.8, 7.5, 10wt%) were prepared. For the Bi containing alloys, the brittle fracture mode appeared showing small amount of reduction of area, while the ductile fracture mode was true for the Bi free alloy. Microstructural examination of ruptured specimens showed cavitations on grain boundaries normal to the load axis, and a significant of grain boundary sliding particularly for the 10wt% Bi alloy. Using SEM, EDS etc., the precipitates inside of and on grain boundaries were identified and their roles in creep strength were explained.

Introduction

Recent worldwide legislative move to ban the use of Pb in consumer electronics triggered intensive research efforts to find materials without toxicity and environmental poisoning as alternatives to conventionally used Pb-Sn eutectic solder[1-3]. The new solder material is supposed to have environmental friendliness, as well as compatibility to the existing manufacturing line, good wettability, good mechanical and electrical property, low cost, and etc. Recently, Sn-3.5Ag eutectic based ternary alloys[4-8] have been gaining wide support from industry, but data on their mechanical properties are rather rare yet. The third elements added to the eutectic include Cu, Bi, In, and Zn[9]. Shimokawa, et al.[10] reported that creep deformation of Sn-57Bi-Ag was dependent on the slip at interfaces between Sn and Bi phases. Vianco, et al[11] studied Sn-3.5Ag-Bi alloys with varying Bi content, and found that hardness leveled off at 5 wt% Bi which was about the solubility limit of Bi in the β -Sn phase. The main strengthening mechanisms were solid solution and precipitation hardening.

In this study, Bi was added to the Sn-3.5Ag eutectic alloy up to 10 wt%, and creep deformation of these alloys under stable microstructures were investigated.

Experimental Procedures

Chemical compositions of Sn-3.5Ag based solder alloys are listed in Table 1 and the nominal composites of Bi was 0, 2.5, 4.8, 7.5, and 10 weight percents (denoted as % hereafter), respectively. In literature, bulk specimens of chill-cast alloys were usually used for the creep studies[12-14]. However, bulk specimen were generally much larger than solder bumps used in real packages, and consequently, microstructures of

specimens were quite different from those of solder bumps. Additionally, as-cast creep specimens usually undergo severe microstructural changes during creep which vary with the applied stress and creep temperatures.

In this experiment, as-cast alloys were cold-rolled about 50%, and dog-bone specimens were machined, and subsequently aged at 393 K for 12 hours to obtain stabilized microstructures. Then, creep testing under constant load were conducted at 373 K and ruptured surfaces were examined.

| Alloy | Sn | Ag | Bi |
|-------|------|------|------|
| 0Bi | 95.7 | 3.61 | - |
| 2.5Bi | 93.7 | 3.57 | 2.51 |
| 4.8Bi | 91.5 | 3.59 | 4.84 |
| 7.5Bi | 88.5 | 3.63 | 7.62 |
| 10Bi | 85.8 | 3.68 | 10.1 |

Tab. 1. Composition of solder alloy. (wt%)

Results

Variations of Vickers hardness are presented as functions of the Bi content in the Sn-3.5Ag alloys in Fig.1. It can be seen that the hardness of as-rolled specimens increase continuously with the Bi content and saturate around 4.8 %Bi. From the Sn-Bi phase diagram[15], the hardness increase seemed to arise from the solid solution strengthening of Bi atoms in the β -Sn matrix, which saturated at the solubility limit. In the case of specimens aged at 393 K, hardness increased above 4.8 %Bi and tended to saturate at 8 %, which was ascribed to the precipitation of Bi particles above the solubility limit. Note that differences of hardness between the 12 hours and 100 hours aging were insignificant at all Bi levels, which suggested the creep under constant microstructures at 373 K. Fig.2 shows X-ray diffraction data of 0, 4.8, and 7.5 Bi alloys, and it can be seen that the 7.5 Bi specimen showed the Bi peak after 12 hrs aging at 393 K, while Bi peaks were not found in the 4.8 Bi specimens. Note that all the specimens showed XRD peaks of Ag_3Sn .

Optical micrographs of specimens with varying Bi contents before creep tests are presented in Fig.3. White and dark areas in Fig.3(a) are Sn matrix and finely dispersed Ag_3Sn intermetallic compounds (IMC), respectively, which were observed under rapid cooling conditions[16][17]. On the other hand, needle-like precipitates observed in 7.5 Bi and 10 Bi alloys were identified as Ag_3Sn . Therefore, addition of Bi to

Sn-3.5Ag resulted in finely dispersed Bi particles and irregularly shaped Ag₃Sn IMC around β -Sn globules[18].

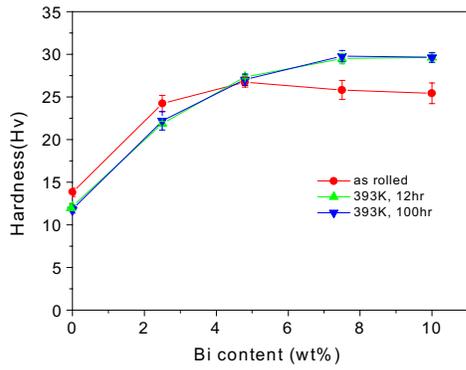


Fig. 1. Hardness of Sn-3.5Ag-xBi alloys with varying Bi content in the as-rolled and heat treated states.

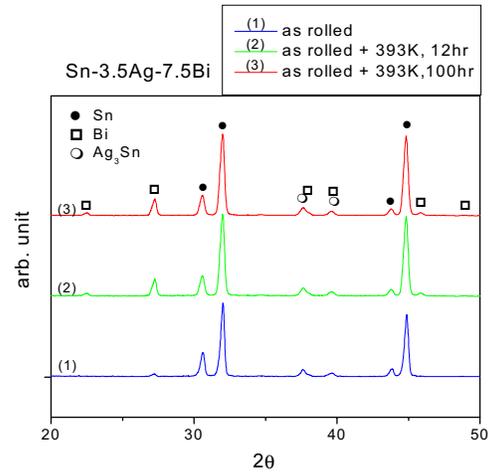
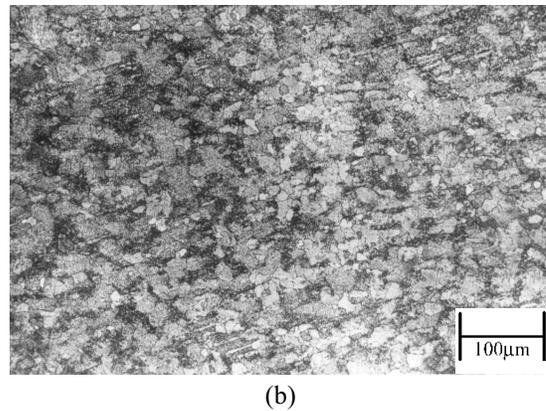
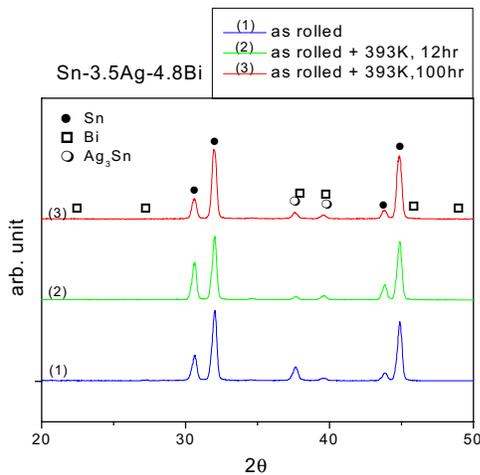
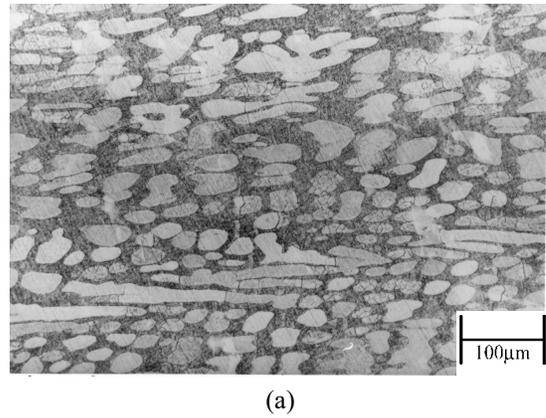
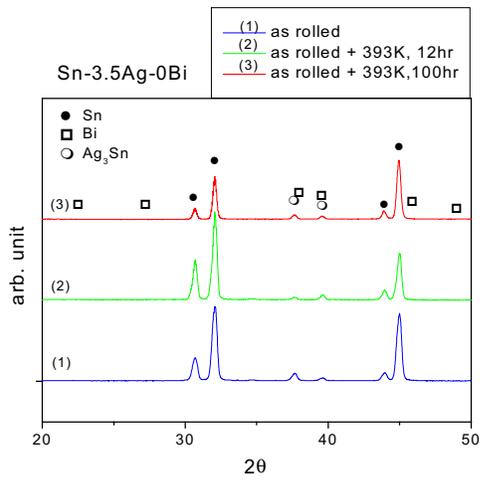
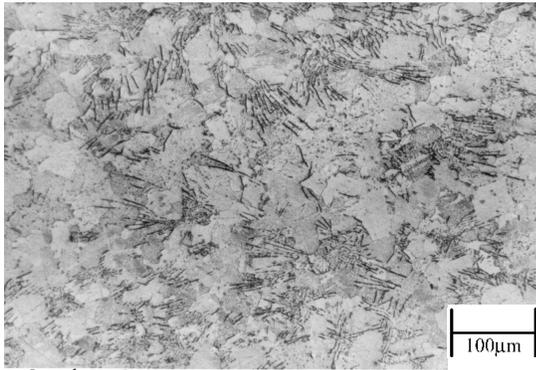


Fig. 2. X-Ray Diffraction of Sn-3.5Ag-xBi specimen.





(c)



(d)

Fig. 3. Optical micrographs of (a) 0, (b) 4.8, (c) 7.5, (d) 10Bi alloys which were annealed for 12 hrs at 393K after rolling.

Creep curves of the Sn-3.5Ag based alloys did not show the primary creep in most cases and the secondary creep ensued immediately after loading, which was followed by the tertiary creep. Minimum creep strain rates are plotted as functions of applied stresses in Fig.4, and it can be seen that the 2.5 Bi alloy showed best creep resistance, while the 10 Bi alloy showed the worst. It appears that Bi atoms in the solid solution below the solubility increased creep resistance slightly, but segregation of Bi to grain boundaries or precipitation of Bi particles in the matrix above the solubility limit deteriorated the creep resistance. Stress exponents of the minimum creep rate, n ($\dot{\epsilon} \sim \sigma^n$) were 4 ± 0.6 except the 10 Bi specimen which showed $n=2$. The stress exponent of $n=2$ was reported in the case of superplastic deformation by grain boundary sliding[19-21]. However, in the case of 10 Bi specimen (ref. Fig.9), brittle creep fracture with the rupture strain of 0.8 was observed, which showed little sign of superplasticity. Grivas[20] observed $n=7$ for the shear stresses greater than 7 MPa, but $n=2$ for the opposite in the Sn/37Pb solder, and ascribed the latter to the superplastic creep by the grain boundary diffusion controlled grain boundary sliding. In the case of Sn-3.5Ag solders, Mavoori[22] reported, $n=11.3$

for stresses between 10 and 22 MPa, which made contrast to $n=5.0$ reported by Mathew[23] for stresses between 3 and 11 MPa. Thus, the present result ($n=4.5$ for the Sn-3.5Ag alloy) showed reasonable agreement to that of Mathew's. Minimum strain rates are plotted as functions of the Bi content at several stress levels in Fig.5. Except the 5.25 MPa data, the steady state creep rate showed minimum at 2.5 %Bi and further addition of Bi deteriorated the creep resistance.

Creep rupture times are plotted as functions of the applied stress in Fig.6, and it can be seen that the rupture time was longest for the 2.5 Bi specimens but shortest for the 10 Bi specimens, as expected. The stress exponent of the rupture time, m ($t_f \sim \sigma^{-m}$) was approximately 5 for the 0 Bi specimens but decreased to 3 for the 10 Bi specimens. In the manner of Fig.5, rupture times are plotted as functions of the Bi content in Fig.7, and it can be seen that rupture time was longest for the 2.5 Bi specimens but decreased with further addition of Bi.

Figure 8 shows the reduction of area (ROA) of ruptured specimens as a function of the Bi content. It can be seen that Bi containing alloys generally showed lower reduction of area than the Bi-free alloy. The 0 Bi specimens showed highest ductility with the tendency of ROA to increase with stress, while 7.5 Bi and 10 Bi showed poorest ductility which was pretty much independent of the applied stress.

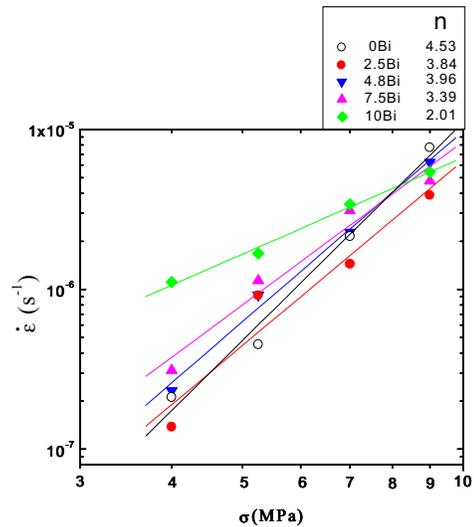


Fig. 4. Minimum creep rates as functions of applied stresses at 373K.

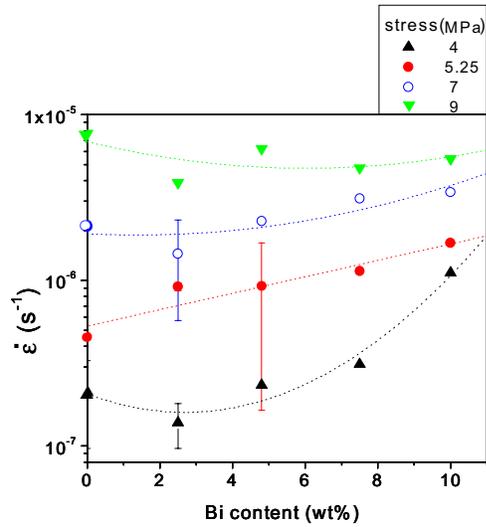


Fig. 5. Minimum creep rates as functions of the Bi content under several stress levels at 373K.

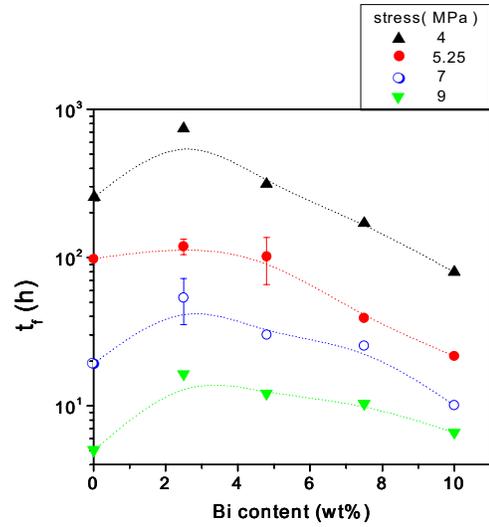


Fig. 7. Rupture time versus Bi content at 373K.

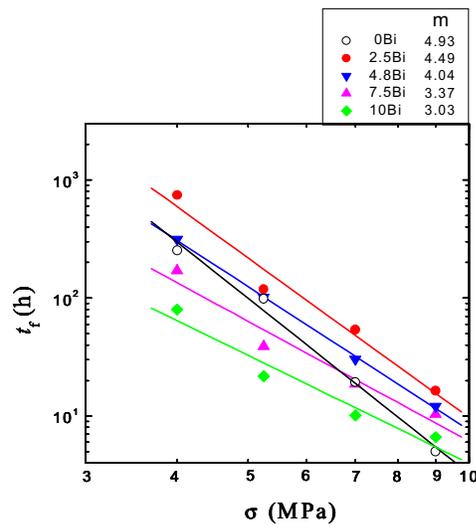


Fig. 6. Rupture time as functions of applied stresses at 373K.

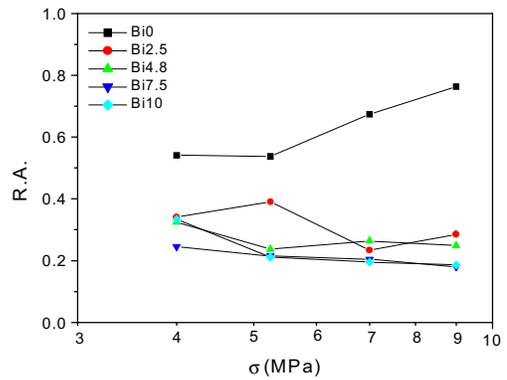


Fig. 8. Reduction of reduction of area vs. the applied stress for various specimens.

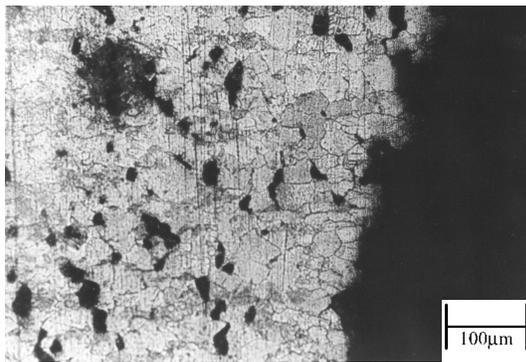
Fig.9 is the optical and SEM micrographs of ruptured 4.8 Bi specimens under several stress levels. Developments of microcracks by the interlinkage of facet sized grain boundary cracks were found, and the grain boundary sliding seemed to assist the linking process under 5.25 MPa. In contrast, the same specimen under 7 MPa showed fewer grain boundary sliding because the creep strain by grain boundary sliding occupied smaller portion of the total strain at higher stress. As can be seen from Fig.9(c), which is an enlarged image of the circled area of Fig.9(b), facet sized single cavities developed instead of numerous cavities at grain boundary precipitates of the facet. Studies on the development and interlinkage of facet sized intergranular cavities are rare in literature. From Fig.9(c),

it seems to be related to the cavity nucleation on bulky Ag_3Sn particles on the grain boundaries, fast grain boundary diffusion, high creep rate, and soft matrix.

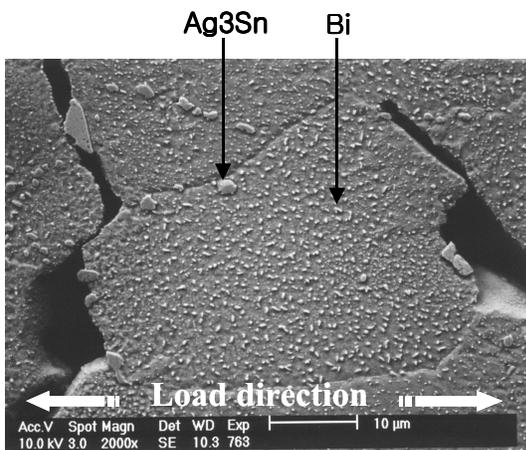
From the above analysis, the creep rupture of Bi containing alloys were concluded to occur by coupled mechanism of high temperature dislocation creep, nucleation and growth of creep cavities, grain boundary sliding and intergranular brittle fracture.



(a)



(b)



(c)

Fig. 9. An optical micrograph of the ruptured 4.8Bi specimen at (a) 5.25 and (b) 7 MPa. (c) An SEM micrograph of the circled region in (b).

Conclusions

1. Creep resistance of the Sn-3.5Ag alloys were best at 2.5 %Bi showing smallest creep rate and maximum rupture time, but deteriorated with more Bi.
2. Creep curves hardly showed primary creep regions, and stress exponents of the minimum creep rate were approximately 4 ± 0.6 except the 10 Bi alloy which showed $n=2$. On the other hand, rupture time showed stress exponents of 3 for the 10 Bi alloy and 4 ± 0.9 for others.
3. Additions of Bi increased the propensity for brittle creep fracture lowering the reduction of area from 0.6 to 0.2.
4. For Bi containing alloys, creep rupture occurred by the mechanism of the high temperature dislocation creep plus nucleation and growth of creep cavities, grain boundary sliding, and intergranular brittle fracture.

Acknowledgments

This study was supported by Center for Electronic Packaging Materials (CEPM) funded by Korea Science and Engineering Foundation (KOSEF).

References

1. J. Muller, H. Griese, and H. Reichl, "Reduced Environmental Impacts by Lead Free Electronic Assemblies? ", ICPworks'99 in Minneapolis, (1999)
2. European Union WEEE Directive, 3rd Draft, May 2000
3. Japanese Ministry of Health and Welfare Waste Regulation, June 1998
4. S. K. Kang and A. K. Sarkhel, "Lead(Pb)-free solders for Electronic Packaging", J. Elect. Mat., Vol.23, No.8, (1994) pp.701
5. S. K. Kang, R. S. Rai, and S. Purushothaman, "Interfacial Reactions During Soldering with Lead-Tin Eutectic and Lead(Pb)-Free, Tin-Rich Solders", J. Elect. Mat., Vol.25, No.7, (1996) pp.1113
6. Judith Glazer, "Microstructure and Mechanical Properties of Pb-Free Solder Alloys for Low-Cost Electronic Assembly: A Review", J. Elect. Mat., Vol.23, No.8, (1994) pp.693
7. M. McCorMack and S. Jin, "Improved Mechanical Properties in New, Pb-Free Solder Alloys", J. Elect. Mat., Vol.23, No.8, (1994) pp.715
8. M. E. Loomans, S. Vaynman, G. Ghosh, and M. E. Fine, "Investigation of Multi-Component Lead-Free Solders", J. Elect. Mat., Vol.23, No.8, (1994) pp.741

9. Y. Kariya and M. Otsuka, "Mechanical fatigue Characteristics of Sn-3.5Ag-X(X=Bi, Cu, Zn and In) Solder Alloys", *J. Elect. Mat.*, Vol.27, No.11, (1998) pp.1229
10. H. Shimokawa, T. Soga, T. Nakatsuka, and K. Serizawa, "Evaluation on the Properties of Sn-Bi-Ag Solder with Low-Melting Point", *ICEP Proc.* 2001, pp.78
11. P. T. Vianco and J. A. Rejent, "Properties of Ternary Sn-Ag-Bi Solder Alloys: Part 1-Thermal Properties and Microstructural Analysis", *J. Elect. Mat.*, Vol.28, No.10, (1999) pp.1127
12. V. I. Igoshev, J. I. Kleiman, D. Shangguan, C. Lock, S. Wong, and M. Wiseman, "Microstructure Changes in Sn-3.5Ag Solder Alloy during Creep", *J. Elect. Mat.*, Vol.27, No.12, (1998) pp.1367
13. J. K. Tien, B. C. Hendrix, and A. I. Attarwala, "Creep-Fatigue Interactions in Solders", *IEEE CHMT*, Vol.12, No.4, (1989), pp.502
14. S. Vaynman, G. Ghosh, and M. E. Fine, "Effects of Palladium and Solder Aging on Mechanical and Fatigue Properties of Tin-Lead Eutectic Solder", *J. Elect. Mat.*, Vol.27, No.11 (1998) pp.1223
15. T. B. Massalski (Ed.-in-chief); *Binary Alloy Phase Diagram*, 2nd ed.
16. R. Darveaux and K. Banerji, "Constitutive Relations for Tin-Based Solder Joints", *IEEE CHMT*, Vol.15, No.6, (1992) pp.1013
17. W. Yang, L. E. Felton, and R. W. Messler, Jr., "The Effect of Soldering Process Variables on the Microstructure and Mechanical Properties of Eutectic Sn-Ag/Cu Solder Joints", *J. Elect. Mat.*, Vol.24, No.10, (1995) pp.1465
18. Y. Kariya and M. Otsuka, "Effect of Bismuth on the Isothermal Fatigue Properties of Sn-3.5Ag Solder Alloy", *J. Elect. Mat.*, Vol.27, No.7, (1998) pp.866
19. M. L. Vaidya, K. Linga Murty, and J. E. Dorn, "High-Temperature Deformation Mechanisms in Superplastic Zn-22Al Eutectoid", *Acta Metallurgica*, Vol.21, (1973) pp.1615
20. D. Grivas, K. L. Murty, and J. W. Morris, Jr., "Deformation of Pb-Sn Eutectic Alloys at Relatively High Strain Rates", *Acta Metallurgica*, Vol.27, (1979) pp.731
21. Z. Mei, D. Grivas, M. C. Shine, and J. W. Morris, Jr., "Superplastic Creep of Eutectic Tin-Lead Solder Joints", *J. Elect. Mat.*, Vol.19, No.11 (1990) pp.1273
22. H. Mavoori, J. Chin, S. Vaynman, B. Moran, L. Keer, and M. Fine, "Creep, Stress Relaxation and Plastic Deformation", *Proc. of Symp. of The Minerals, Metals & Materials Society*, (1997)
23. M. D. Mathew, Sashidhar Movva, Hong Yang, and K. Linga Murty, "Creep of Sn, Sn-3.5Ag and Sn-5Sb Solders for Electronic Packaging", *Proc. of Symp. of The Minerals, Metals & Materials Society*, (1999)